ISSN 0010-9525, Cosmic Research, 2006, Vol. 44, No. 4, pp. 364–383. © Pleiades Publishing, Inc., 2006.
Original Russian Text © L.V. Zasova, V.I. Moroz, V.M. Linkin, I.V. Khatuntsev, B. S. Maiorov, 2006, published in Kosmicheskie Issledovaniya, 2006, Vol. 44, No. 4, pp. 381–400.

Structure of the Venusian Atmosphere from Surface up to 100 km

L. V. Zasova, V. I. Moroz†, V. M. Linkin, I. V. Khatuntsev, and B. S. Maiorov

Space Research Institute, Russian Academy of Sciences, Profsoyuznaya ul. 84/32, Moscow 117997, Russia

Received April 7, 2006

Abstract—The goal of this paper is to summarize the experimental data on the atmosphere of Venus obtained after 1985, when the VIRA (Venus International Reference Atmosphere) or COSPAR model was published. Among the most important results that have appeared since then are the following: measurements of the vertical temperature profile by the *VEGA* spacecraft with high precision and high altitude resolution; measurements made with balloons of the *VEGA* spacecraft; radio occultation measurements of *Magellan*, *Venera-15*, and *Venera-16*; and temperature profiles derived from the data of infrared spectrometry obtained by *Venera-15*. The new result as compared to VIRA is the creation of a model of the atmosphere in the altitude range 55 to 100 km dependent on local time. This model is presented in our paper in tabulated form.

PACS numbers: 96.30.Ea

DOI: 10.1134/S0010952506040095

INTRODUCTION

In total, 15 Soviet and 7 American missions have been studied Venus starting from 1962. Chronology of these events is described in [1–2]. These studies were most extensive in 1960s and 1970s. It is worthwhile to mention the American flyby spacecraft *Mariner-2*, *Mariner-5*, and *Mariner-10*; the Soviet flyby stations *Venera-4* to *Venera-8* and *Venera-11* to *Venera-14*; orbital stations *Venera-9* and *Venera-10* having delivered landing modules; and the American mission *Pioneer Venus* that included both an orbital spacecraft and descent probes. As a result of this exploration activity, a large body of data was obtained. The data concerning the atmosphere were classified and collected in Venus International Reference Atmosphere (VIRA).

VIRA was published in *Advances in Space Research* in 1985 [3]. The first chapter of VIRA is dedicated to the thermal structure of the atmosphere at altitudes lower than 100 km [4].

In 1980s and 1990s Venus was studied not so extensively, however, some spacecraft have got important data about the Venusian atmosphere. In 1983 the *Venera-15* orbital station explored the planet using a Fourier spectrometer (FS) for the thermal infrared spectral range [5–7]. In case of *Venera-15* and *Venera-16*, both spacecraft also obtained some data as a result of radio occultation of the atmosphere of Venus [8–10]. During the 1985 *Vega-1* and *Vega-2* missions the landing vehicles and balloons were delivered to Venus [11–13]. The *Galileo* spacecraft having passed by Venus in 1990 made measurements in the near infrared range (experiment NIMS), as a result of which important data were obtained concerning the atmosphere and lower cloudy layer on the night side of Venus [14–18]. Ground-based observations of the night side of Venus yielded a lot of data about the subcloud atmosphere [19–21]. Radio observations made by the *Magellan* mission in the beginning of 1990s gave several profiles of temperature and density from 35 to 95 km [22]. The last observations of the night side of Venus from spacecraft were carried out recently by the *Cassini* mission (VIMS experiment) [23].

Below, we list the most important data obtained in these experiments that can be used to improve the VIRA model from the surface to a height of 100 km.

(1) The temperature profile from the surface up to 12 km height which was first obtained with sufficient accuracy by the *VEGA-2* landing module (all descent modules of *Pioneer Venus* were switched off at the height of 12 km, while no measurements of preceding *Venera* missions can be considered accurate enough).

(2) Horizontal variations of temperature and pressure that were found as a result of experiments with balloons *VEGA-1* and *VEGA-2*.

(3) The temperature profiles derived as a result of interpretation of the IR Fourier spectrometer measurements onboard *Venera-15*, which allowed one to construct a time-dependent model of the middle atmosphere for altitudes of 55–100 km and to get the distribution of amplitudes for a thermal tide as a function of latitude and altitude.

(4) Radio occultation experiment on *Venera-15* and *Venera-16* which allowed one to derive temperature profiles in the interval of heights 40–80 km.

† Deceased.

Table 1

	φ°	λ°	LT, h	P_{min}	P_{max}, mbar	T_{min}, K	T_{max}, K	H_{min}, km	H_{max}, km
VEGA-1	8 N	77	0.3	540	630	308	322	53	54
VEGA-2	7.5 S	180	1.0	535	900	302	338	50	54

(5) Radio occultation experiment on the *Magellan* orbiter which allowed one to reconstruct several temperature profiles with sufficient accuracy and a high spatial resolution.

The original VIRA model was constructed on the basis of a huge body of data accumulated before 1985, when extensive space exploration of Venus was carried out. So, it represents a complete review of all data available at that time. We are not going to analyze these data once again; we will present only those new results which can supplement the model retaining the structure of the original VIRA model.

STRUCTURE OF THE ORIGINAL VIRA MODEL

The atmosphere of Venus from the surface up to a height of 100 km includes the lower atmosphere ($H <$ 50 km) and the middle atmosphere in the interval from 50 to 100 km (the boundaries are conventional). Sometimes, the level of 60 km is taken as a boundary between the middle and lower atmosphere, which is close to the mean value of the tropopause altitude derived from the radio occultation measurements made by *Pioneer Venus*, *Venera-15*, and *Venera-16* [9, 24].

In the VIRA model the atmosphere from 0 to 100 km are divided in three layers: 0–40 km, 40–60 km, and 60–100 km. These three layers differ both in methods of their exploration and in physical conditions inside them: only direct measurements are available for the first layer, the second layer admits radio occultation in addition to direct measurements, and for the third layer the radio occultation, accelerometry, and IR-spectrometry are available. Here we retain this partition and recall the main characteristics of these layers of the atmosphere included in VIRA.

Lower atmosphere for altitudes h < 40 km

The model of the atmosphere in this interval was constructed on the basis of measurements made by the descent modules of *Venera-10–Venera-12* and *Pioneer Venus*. Below 12 km only the measurements made by *Venera-10* were available, and the model of this layer was based on them. A typical scatter of temperature profiles obtained in various experiments is a few degrees. It is a consequence of difference in latitude, local time, and amplitudes and phases of gravity waves at the landing place. However, these data are not sufficient in order to derive the temperature dependence on latitude or local time. Taking into account that variations of temperature obtained in different experiments are small, for the sake of simplicity, a single model of the atmosphere structure in this altitude region was accepted. However, one should note that local temperatures can differ from the model values by up to 10 K, though most typical variations are 5 K. The lower atmosphere is stable against convection excluding the altitude range 20–30 km and a layer near the surface.

The atmosphere in the altitude range 40–60 km

The model is based on measurements with descent modules and on the radio occultation data obtained by *Pioneer Venus*. As a result of radio occultation the atmosphere profiles were derived for different latitude zones, which allowed one to construct a latitude-dependent model: five latitude zones were selected: $\varphi < 30°$, $\varphi = 45°$, $\varphi = 60°$, $\varphi = 75°$, and $\varphi = 85°$. The atmosphere is stable in this altitude range with an exception of $h =$ 50–57 km (the middle cloudy layer).

Middle atmosphere in the altitude range 60–100 km

The data of three types of experiments were included in the model: (1) temperature profiles obtained as a result of the Infrared Radiometer (OIR) experiment onboard *Pioneer Venus*; (2) profiles of the atmosphere according to radio occultation by *Pioneer Venus*; and (3) the results of accelerometric experiments onboard *Pioneer Venus* and in *Venera* missions. Five altitude profiles of temperature, pressure, and density were constructed for the latitude zones specified above. One can notice that the mean temperature in the equatorial atmosphere varies with longitude in a solar-bounded way, which is described by a half-day wave of the thermal tide. Periodic variations are described both for the cold collar (a period of 5.9 days) and for the hot dipole (2.9 days period).

The VIRA model includes the tables of vertical structure of the atmosphere (temperature T, pressure P, density D, and some auxiliary parameters). The lower atmosphere model is constructed under an assumption that there are no latitude or synoptic variations (Tables 1-1 in paper [4] for altitude intervals of 0–32 km). The middle atmosphere model (Tables 1-2 in the same paper for an interval of 33–100 km) includes latitude variations.

Data Sources for Upgrading the Model

In what follows we, retaining the structure of the original VIRA model, consider how the data obtained later agree with the existing model and what new could

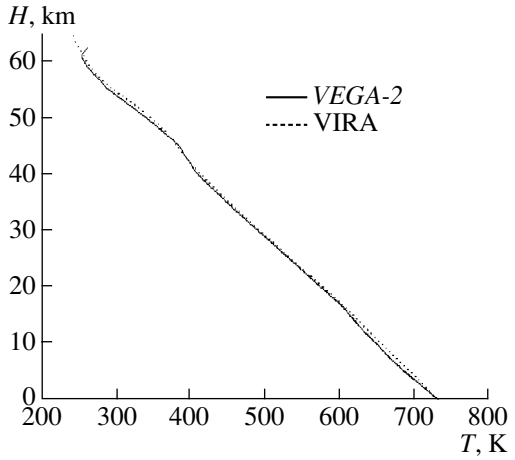

Fig. 1. Temperature profiles measured by the *VEGA-2* descent module (solid line) in the altitude range 0–63 km and a model temperature profile of VIRA (dotted line).

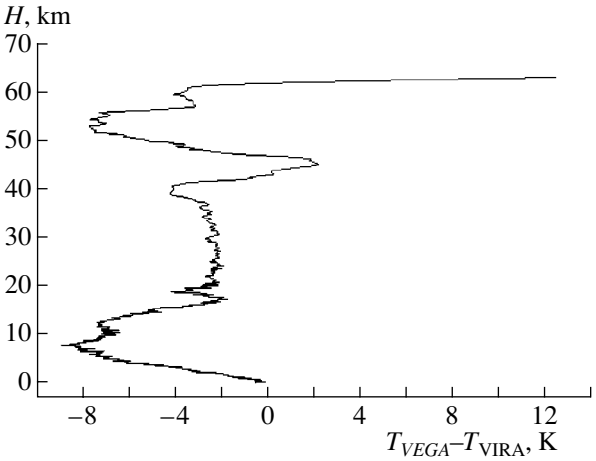

Fig. 2. The difference between the temperature profile measured by the *VEGA-2* descent module and that of VIRA model.

be derived from them for model improvement. Now let us remind which data have appeared since 1983.

(1) A meteorological experiment on the *VEGA-2* descent module (below an altitude of 62 km).

(2) Meteorological experiments on balloons *VEGA-1* and *VEGA-2* (51–55 km).

(3) Radio eclipse measurements conducted by *Magellan*, *Venera-15*, *Venera-16*, and later measurements by *Pioneer Venus* (40–80 km).

(4) Infrared spectrometry on *Venera-15* (55–100 km).

(5) NIMS (*Galileo*) and ground-based microwave measurements (70–90 km).

From the data listed above we do not use below the *Galileo* NIMS temperature profiles obtained in the wavelength range 4.3 μm and microwave measurements in CO lines (70–90 km), since they have low resolution and add nothing new in comparison with the data of infrared spectrometry and radio occultation experiments.

MODEL OF THE LOWER ATMOSPHERE

Since the time of VIRA publication the meteorological measurements have been made by the *VEGA-2* spacecraft (1984) in the lower atmosphere of Venus: new temperature and density profiles were measured from 62 km down to the surface [11–12]. The vertical profiles of temperature and pressure have higher accuracy than those obtained by preceding *Venera* missions. The accuracy of determination of the temperature profile is ~1 K. Below 12 km the vertical profiles of pressure and temperature were obtained for the first time with sufficient accuracy by *VEGA-2* spacecraft. There are detailed tables in [12]. We present in Figs. 1 and 2 a comparison of the temperature profile measured by *VEGA-2* with the model temperature profile of VIRA. Notice that, generally, a good agreement of the profiles prevails. However, there are also some distinctions, especially well seen for altitudes lower than 15 km and higher than 58 km. The difference between the measured and model temperature profiles is presented in Fig. 2. The measured temperature is systematically lower excluding a narrow interval of altitudes around 45 km and a layer above 60 km, where inversion appears in the temperature profile of the *VEGA-2* spacecraft.

The largest difference between the profiles is observed at altitudes of about 8 km (where the temperature measured by *VEGA* is lower by 9 K than the model one) and about 63 km (where the difference exceeds 13 K). The distinction between the profiles below 10 km can be attributed to inaccuracy of the VIRA data that are based on a single profile measured by *Venera-10* and on extrapolation of the profiles obtained by *Pioneer Venus* probes (they were switched off at an altitude of 12 km). This distinction can also be assigned to real variations of temperature which are not excluded even in the lower atmosphere. The temperature difference value is within the limits of possible local variations, as they are recorded in VIRA.

The profile of static stability was calculated on the basis of the *VEGA* spacecraft temperature profile [12] with subsequent comparison with VIRA (Fig. 3). The measured profile is in a good agreement with the model one: the atmosphere is basically stable excluding two intervals of altitudes: 49–55 km (the middle and lower cloud layers) and the layer between 18 and 30 km. The peak of stability (even better pronounced than in VIRA) is observed near the altitude of 15 km. Below this peak, the atmosphere is virtually stable down to the surface, if one proceeds from the assumption of model profile, while for the measured profile an instability is possible in the layer between 2 and 4 km.

TEMPERATURE PROFILES IN THE ALTITUDE RANGE OF 40–60 KM

Several measurements are available for this interval of altitudes: made by the *VEGA-2* spacecraft, with balloons *VEGA-1* and *VEGA-2*, and radio occultation measurements made in orbit by *Magellan*, *Venera-15*, *Venera-16*, and *Pioneer Venus*.

VEGA Data

For this interval of altitudes one can compare the temperature profiles obtained by the *VEGA-2* with VIRA in Figs. 1 and 2. The largest difference (–8 K) is observed in the altitude interval 52–57 km in the middle cloud layer. Below the clouds, from 40 to 48 km of altitude, the difference between profiles varies from –2 to + 4 K.

Balloon measurements of *VEGA-1* and *VEGA-2* were carried out during their 40-h floating flight in the middle cloud layer of the atmosphere of Venus [13]. They covered the interval of local time from midnight up to 08 LT, the total rout passed by balloons in the atmosphere being about 11000 km long. The *VEGA-1* balloon moved along the parallel of latitude 8° north. The trajectory of *VEGA-2* balloon was shifted along the meridian by 500 km to the south. The extreme values of temperature and pressure along the balloon routs are presented in Table 1.

Complete data on temperature and pressure along the balloon routs can be found in [11]. For both balloons the pressure dependence of temperature turned out to be close to adiabatic, the adiabatic lines being displaced by several Kelvins. This was interpreted as an indication to existence of sufficiently extended nonmixing atmospheric masses. Each balloon during the flight was inside its own region of this type.

Paper [13] presents the values of static stability along the trajectories. The *VEGA-1* balloon was flying in a more stable region (the quantity d*T*/d*H* varied from 0 to + 2.5 K/km), while the *VEGA-2* balloon encountered with a sharp instability, especially in the beginning of measurements.

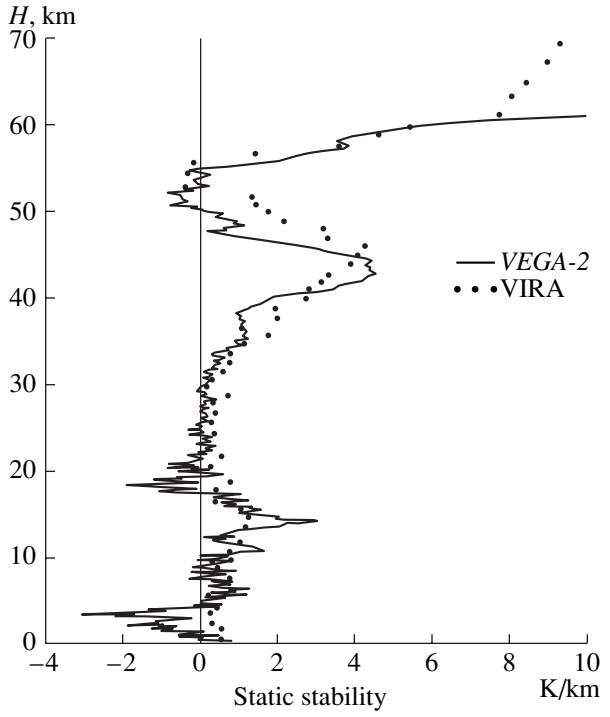

Fig. 3. The profile of static stability derived from *VEGA-2* temperature profile (solid line) in comparison with the model VIRA profile (dots).

RADIO ECLIPSE MEASUREMENTS

Radio Eclipse Measurements Made by Magellan

Radio eclipse (RE) experiments give a possibility to get temperature profiles in the altitude range from 40 km to 80–90 km. The last spacecraft on whose board the radio occultation measurements were conducted was the American spacecraft *Magellan*. Its three temperature profiles are presented in [22] together with corresponding profiles of static stability.

The temperature profiles obtained by *Magellan* have better spatial resolution than those measured previously in radio occultation experiments onboard *Pioneer Venus*, *Venera-15*, and *Venera-16*. However, *Magellan* obtained only a few vertical profiles which could not provide for any significant coverage in latitude and local time. The temperature profiles [22] have a wavelike form which is, apparently, explained by the action of gravity waves. The profiles of static stability show the atmosphere to be stable against convection above the middle cloud layer (higher than 57–60 km). It follows from all three profiles that the atmosphere is convectively unstable (or close to this state) in the altitude range 50–57 km, i.e., in the middle cloud layer. All these conclusions are in a good agreement with the data of *VEGA-1* and *VEGA-2* and with the static stability profile of VIRA.

Several temperature profiles for comparison were kindly put at our disposal by Dr. J. Jenkins. We use below the following designations: VIRA 30 (45, 60, 75, 85) is the VIRA model for a specified latitude; M 56–14N are RE measurements by *Magellan* with latitudes of their beginning and end. A specific feature of RE profiles is the fact that their different parts (at different altitudes) of one and the same temperature profiles can belong to different latitudes. This is valid for almost all *Magellan* profiles, higher levels in the atmosphere being in correspondence with higher latitudes. The only exception is temperature profiles for the southern polar region. Therefore, we designate the *Magellan* temperature profiles with specifying the latitude range of observations. For example, in M 56–14N the first number is the latitude relevant to higher levels of 80–90 km, while the second number is the latitude corresponding to the lowest levels (35–40 km).

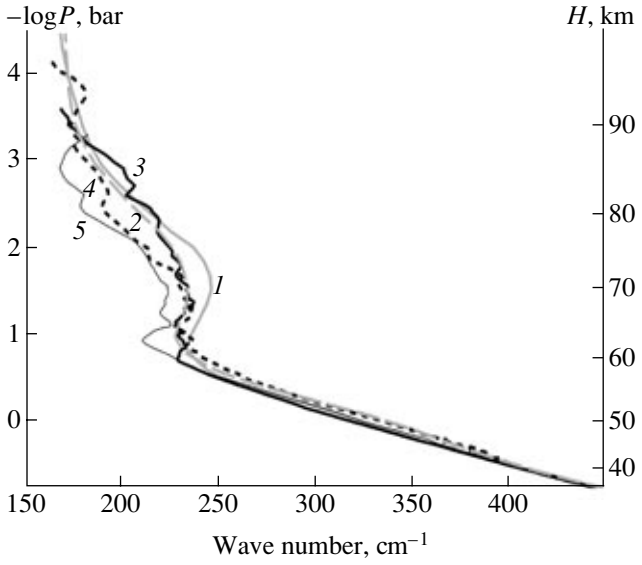

Fig. 4. *Magellan* temperature profiles as compared to the model for corresponding latitudes: (*1*) VIRA 60, (*2*) VIRA 75, (*3*) M 77–65N, (*4*) M 68–58N, and (*5*) M 69–34S.

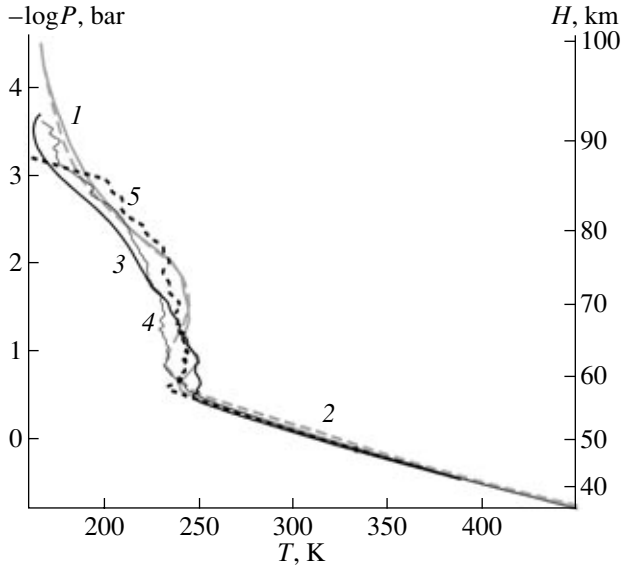

Fig. 5. The same as in Fig. 4, but for the polar region: (*1*) VIRA 85 (solid gray line), (*2*) VIRA 75 (dashed gray line), (*3*) M 88–86S (LT = 00), (*4*) M 83–77N, and (*5*) M 88–88S (LT = 6 AM).

Figure 4 presents a comparison of three temperature profiles obtained by *Magellan* for middle latitudes with corresponding VIRA models, and Fig. 5 compares with VIRA three temperature profiles of the northern and southern polar region. One can note that the difference of temperature measured by *Magellan* and the model is in the interval 0–7 K, which is within the limits of possible local variations.

Radio Eclipse Experiments onboard Spacecraft Venera-15 and Pioneer Venus

In October–November 1983 radio occultation observations were made by *Venera-15* and *Venera-16* (RE V15). In papers [8–10] 26 profiles of the neutral atmosphere are described. The temperature profiles averaged over the latitude zones 82°–88° S, 60°–75° S, 81°–86° N, and 74°–79° N are published in the tabulated form (the authors refer to them as southern polar, southern near-polar, northern polar, and northern near-polar regions, respectively). Let us designate them as SP, SNP, NP, and NNP, respectively. The temperature profiles for these regions are presented in Fig. 6 together with model profiles VIRA 75 and VIRA 85. Lower than 60 km the temperature derived as a result of RE V15 for near-polar northern and southern regions exceeds the model temperature VIRA 75, and this difference lies within the limits 0–13 K. For both polar regions the temperature derived from RE V15 turns out to be lower by 0–5 K than the model temperature VIRA 85.

The height and temperature at the tropopause level obtained in the experiments onboard *Venera-15* and *Venera-16* are given in paper [10]. On the average, the tropopause level height varies from 58.5 km in the latitude region 80°–90° up to 62.5 km at latitudes of 60°–70°. For individual measurements the range of variation of the tropopause level height is from 56 to 64 km. Temperature at this level lies within the limits 200–260 K.

The radio occultation experiment onboard *Pioneer Venus* determined the location of the tropopause level

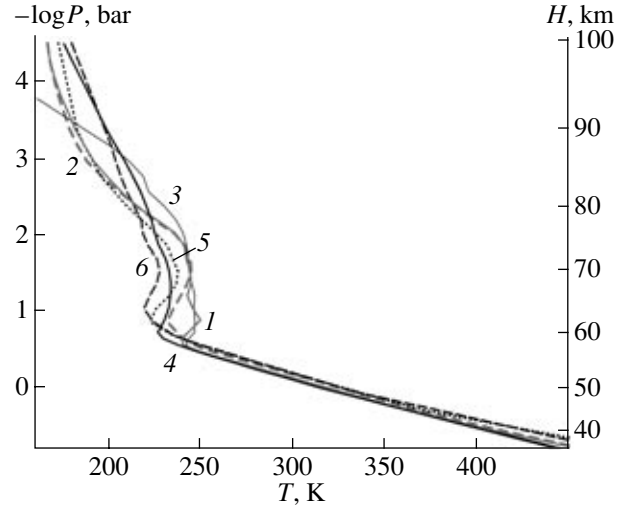

Fig. 6. Temperature profiles obtained during the *Venera-15* radio occultation experiment in comparison with VIRA models for corresponding latitudes: (*1*) VIRA 85 (solid gray line), (*2*) VIRA 75 (dashed gray line), (*3*) RE V15 NP, (*4*) RE V15 SP, (*5*) RE V15 NNP, and (*6*) RE V15 SNP. The right Y axis presents altitudes calculated using $h(p)$ dependence for VIRA 75.

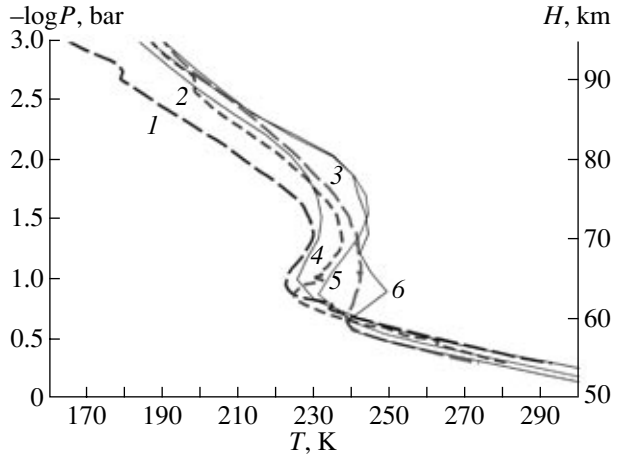

Fig. 7. The same as in Fig. 6, but the results of RE experiments of *Pioneer Venus* are compared with VIRA: (*1*) ORO PV 60, (*2*) ORO PV 75, (*3*) ORO PV 85, (*4*) VIRA 60, (*5*) VIRA 75, and (*6*) VIRA 85.

from the equator up to the pole [24]. In the latitude range 60°–90° the data obtained [10] are in a good agreement with previously published data [24]. For lower latitudes ($\varphi < 60°$) the tropopause level height decreases reaching a minimum value of 55 km in the equatorial region (*Pioneer Venus*).

The radio occultation experiment onboard *Pioneer Venus* [25] continued until 1992. Three series of measurements were made at varying solar activity: at high solar activity in 1978–1983 (below, this period is referred to as OROHI78); in 1984–1986 a series of measurement was made at low solar activity (OROLO84); and in 1989–1992 again at high solar activity (OROHI89). Dr. A. Kliore kindly put the data for comparison at our disposal. In Fig. 7 we present the averaged temperature profiles together with VIRA model profiles for corresponding latitudes.

Altitude Dependence of Pressure

We have made a comparison of the altitude dependence of pressure as measured in radio occultation experiments by *Magellan*, *Venera-15*, and *Venera-16* with the data published in the VIRA model for corresponding latitudes.

For northern and southern polar regions the vertical profiles of pressure were obtained by both *Magellan* and *Veneras*. The profiles of altitude dependence of pressure for both polar regions are presented in Fig. 8a. Two upper curves present the data of RE V15, while two lower curves represent the profiles obtained by *Magellan*. Obviously, below 60 km there is a good agreement between the curves for both polar regions inside a single experiment, and a systematic difference takes place between different experiments: *Magnellan* systematically gives the higher values of pressure.

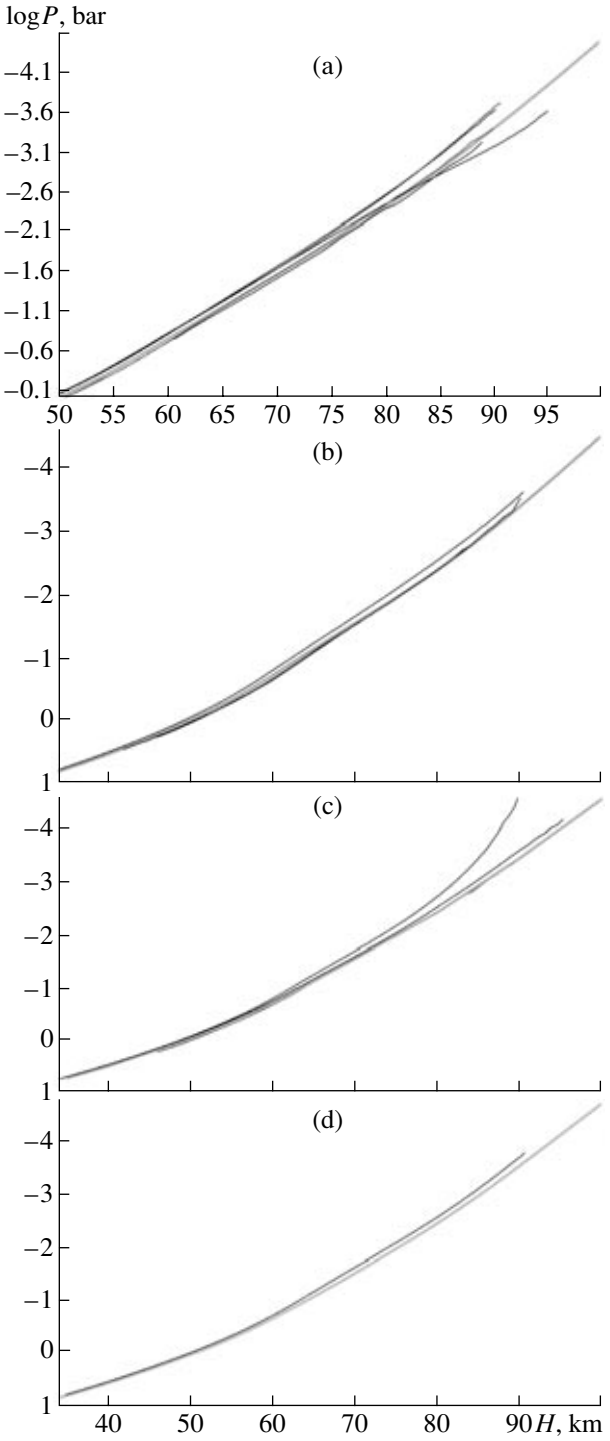

Fig. 8. (a) Vertical pressure profiles obtained in RE experiments onboard *Venera-15*, *Venera-16*, and *Magellan* in the polar region in comparison with the VIRA 85 model. The middle (gray) curve is for VIRA 85, two lower curves represent RE V15, and three upper curves are for M 88–88S, M 82–77N, and M 88–87S. (b) The same as in Fig. 15, but for near-polar regions. The middle (gray) curve is for VIRA 75, two lower virtually coinciding curves are for RE V15, and the upper curve is for M 77–65N. (c). The same as in Fig. 15, but for M 69–35S (upper curve), M 67–58N (middle curve), and VIRA 60 model (gray curve). (d) The same as in Fig. 15, but for M 56–15S and VIRA 45 model (gray curve).

The curve of altitude dependence of pressure in VIRA model lies between the curves of two experiments and is close to their averaged values. For example, the pressure at an altitude of 50 km is equal to 0.938, 1.022, and 1.119 according to the curves for RE V15, VIRA 85, and *Magellan*, respectively (Fig. 8a). The systematic difference between experiments can also be caused by real variations of pressure. Thus, one can regard the accuracy of VIRA model for $P(H)$ dependence to be not worse than 10%.

For the sake of comparison with model VIRA 75 for the near-polar region one can use the measurements of *Venera-15* and *Venera-16* for both hemispheres and one profile obtained by *Magellan* for the northern near-polar region. The vertical profiles of pressure for near-polar regions are presented in Fig. 8b.

Below the level of 70 km the curve constructed according to the VIRA model also lies between the curves obtained by RE V15 and *Magellan*, however, above 70 km the model curve approaches the curve RE V15. Notice that the vertical profile of pressure derived from RE V15 coincides for the northern and southern near-polar regions. The RE experiment onboard *Magellan* gives systematically higher values of pressure, including the case of near-polar region.

Let us compare now the *Magellan* vertical profiles of pressure M 69–35S and M 56–15N with VIRA 60 and VIRA 45 profiles (Figs. 8c and 8d, respectively).

It follows from the figures presented above where the vertical profiles of pressure are compared that the *Magellan* pressure values exceed the values presented in VIRA for all analyzed profiles for corresponding latitudes and altitudes. Thus, RE experiments give systematically lower values of pressure virtually in all cases under analysis. Systematic difference between these experiments is either due to temporal and local variations or a result of systematic errors.

MODEL OF THE MIDDLE ATMOSPHERE OF VENUS FROM 60 TO 100 KM

In order to upgrade the VIRA model for the middle atmosphere region, now more complete data are available. Among them are the following experiments: *Magellan* RE measurements; *Venera-15* and *Venera-16* observations; *Pioneer Venus* data; and temperature profiles obtained onboard *Venera-15*.

The direct measurements onboard the *VEGA-2* descent module started from an altitude of 62 km, i.e., they also give some information about the lowest layers of the middle atmosphere in the equatorial region. Inversion in the temperature profile (Fig. 1) was discovered at altitudes higher than 60 km. This inversion can be a narrow local peculiarity. However, the temperature profile presented in paper [8] according to RE V15 has a similar inversion at close altitudes.

Radio Eclipse Experiments

Magellan. Radio eclipse experiments give vertical profiles of temperature, density, and pressure up to altitudes of 80–90 km. In order to describe the profiles derived, we return to Figs. 4 and 5, where one can compare *Magellan* measurements with corresponding VIRA models. Measured temperatures for the near-polar region are lower than VIRA 75 at $h < 75$ km, with a peak deviation of 17 K about 70 km. At $h > 80$ km they are higher than VIRA. For both polar regions (northern and southern) temperatures in the VIRA 85 model are higher, as a rule, than the measured temperature, excluding the regions near 60 km and in the altitude interval 80–85 km. Again, we draw attention to the altitude interval 65–75 km, where the distance reaches its maximum. The temperature obtained by *Magellan* has a wave-like form above 60 km, and, presumably, gravity waves are responsible for this fact.

Venera-15 and Pioneer Venus. The temperature profiles for the northern and southern polar and near-polar profiles are presented in Fig. 6. Higher than 75–80 km measured temperatures are higher than model temperatures for all polar and near-polar regions. In the altitude interval 60–75 km the difference between VIRA 85 and NP V15 lies within the limits –5 to + 3 K. Three other temperature profiles of RE V15: SP, NNP, and SNP demonstrate lower temperatures as compared to the VIRA model. The difference is 10 K for NNP and reaches 20 K for SP and SNP regions. Figure 7 presents a comparison of later measurements by *Pioneer Venus* (averaged for the latitude zones used in VIRA) with corresponding model temperature profiles. It is worth noting that temperatures in the *Pioneer Venus* profile for $\varphi = 60°$ are systematically lower, with a difference exceeding 10 K above 70 km.

In conclusion, we may say that in polar and near-polar regions RE experiments of both *Magellan* and *Venera-15* regularly give lower temperatures than the model in the altitude interval 60 to 75 km (the only exception is RE V15 temperature profile for the NP region).

Figure 9a presents the difference between temperature profiles VIRA 85 and experimental temperature profiles in the polar region, including both radio occultation results and obtained by infrared spectrometry onboard *Venera-15*. All curves have a similar form between 60 and 75 km, and positive difference reaches 20 K.

For near-polar regions (Fig. 9b) the difference between VIRA 75 and experimental profiles in the altitude range 65–75 km has a character similar to that shown in Fig. 9a, but with a somewhat less value of the difference. One can conclude that VIRA 85, as well as VIRA 75, gives the temperatures exceeding measurement values in the altitude range 60–75 km by up to 20 K. It seems that model temperature profiles VIRA 85 and VIRA 75 require corrections in the altitude range 60–75 km.

Infrared Spectrometry onboard Venera-15

The biggest increase of the amount of data that has took place since VIRA publication is associated with infrared spectroscopy made by *Venera-15* [5–7]. About 2000 spectra were taken in the wavelength range 6–40 μm. The 15 μm spectral profiles of CO_2 band and the spectral intervals free from gas absorption were used for reconstruction of vertical profiles of temperature and aerosol distributions in the altitude interval 55–100 km [27–35]. Most of the observations span the latitude range from 20° to 87° N. The equatorial and southern (up to 65° S) regions were observed during a special run. *Venera-15* operated in the near-polar orbit, therefore, a wide range of latitudes was surveyed virtually simultaneously and almost at one and the same local time (between 03:30–10:30 LT and 16:30–22:30 LT). During measurements near the pericenter the size of the field of view was about 60 km.

We have used temperature profiles in the altitude interval 58–100 km. The lowest level to which temperature can be reconstructed depends on the structure of the upper level of clouds. The upper cloud level is inhomogeneous in the thermal infrared range, especially at high latitudes: in the most transparent spectral region of continuum (about 365 cm^{-1}) the optical thickness reaches unity at altitudes of 55 to 59 km depending on latitude and local time. Therefore, for purposes of this work, in order to have homogeneous data for averaging, we restricted ourselves to the level of 58 km. We have made interpolation downward in order to reach at a level of 50 km the temperature corresponding to the VIRA model [4] at a given latitude.

During the equatorial run the measurements were conducted at 07:30 LT. Approximately at the same local time (07:38 LT) five years later the *Pioneer Venus* probe obtained a temperature profile *in situ* at latitude 4° N. The field of view of the Fourier spectrometer at equatorial measurements equaled about 500 km. Due to this reason, the data were averaged over 5 degrees of latitude. In Fig. 10 the temperature profile FS V15 is compared to that measured by *Pioneer Venus*. One should have in mind that *Pioneer Venus* profiles are characterized by significantly higher spatial and vertical resolution. Nevertheless, a reasonable agreement is observed between the temperature profiles (see, for example, the location of the region of local temperature inversion above 80 km in morning hours).

In Figs. 11a–11c the averaged temperature profiles FS V15 is compared with the model for corresponding latitude zones. Correlating morning (*2*) and afternoon (*3*) temperature profiles one can see that afternoon temperature is lower at altitudes above 85 km and higher in the interval 75–85 km, at altitudes less than 75 km it becomes lower again. One can notice that VIRA 30 on the average describes satisfactorily thermal structure of the atmosphere at low latitudes.

As is shown by the *Pioneer Venus* OIR experiment, the radiation field of Venus is very inhomogeneous in the thermal spectral range. At high latitudes, infrared details are well pronounced, such as the cold collar and hot dipole. A description of the spectra of the infrared details can be found, for example, in [32]. In Fig. 11b the temperature profiles in the near-polar region are compared with temperature profiles VIRA 60 and VIRA 75. The profiles are averaged over the coldest region of the cold collar (*3*) observed on the morning side and over the warmest regions on the same latitude (*4*) observed in the afternoon. The form of temperature profile VIRA 60 is well consistent with the profile form for warm regions in the interval 55°–75°. At higher latitudes the warm regions belong to the hot dipole. The

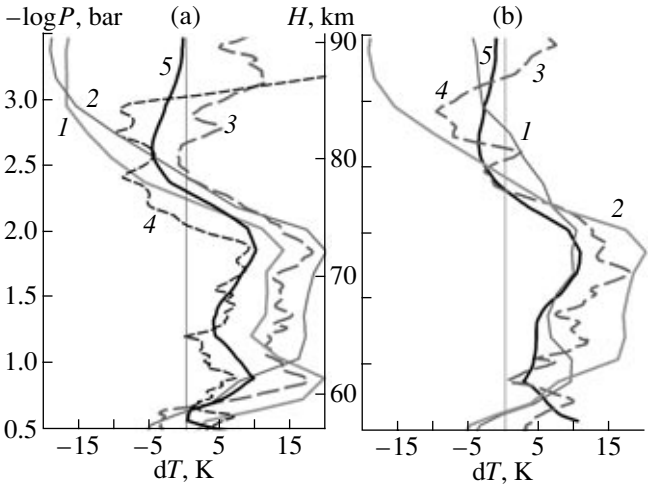

Fig. 9. Difference between model and experimental temperature profiles for the northern and southern polar (a) and near-polar (b) regions. (a) Difference between VIRA 75 and (*1*) RE V15 SNP, (*2*) RE NNP, (*3*) M 77–65N, and (*4*) IR V15 (65–85 N); (b) difference between VIRA 85 and (*1*) RE V15 SNP, (*2*) RE NNP, (*3*) M 88–86S, (*4*) M 83–78N, and (*5*) IR V15 (φ > 85° N).

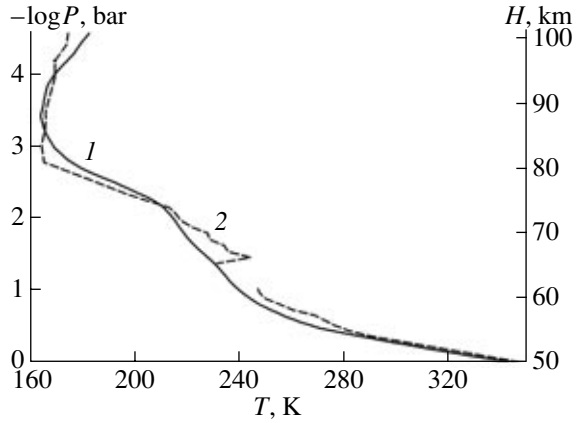

Fig. 10. Reconstructed temperature profile IR V15 (*1*) averaged in the interval 0–5° N for 7: 30 AM compared with the profile (*2*) derived from measurements made by *Pioneer Venus Sounder* probe (in 4° N latitude at 7:38 AM of local time) [36].

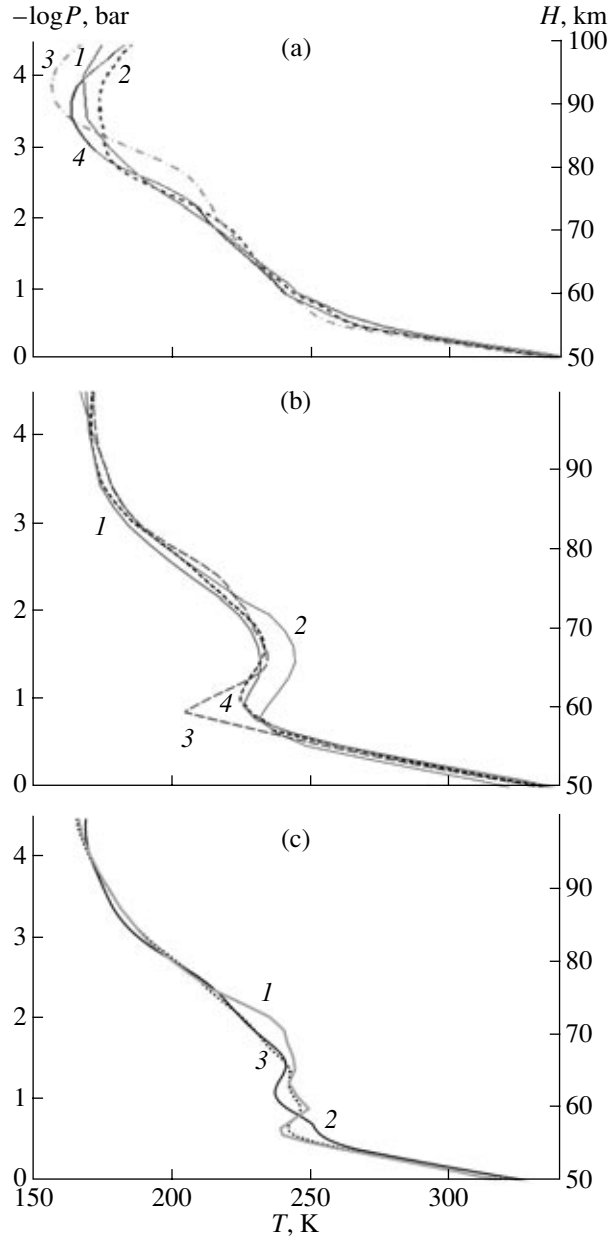

Fig. 11. (a) Temperature profiles VIRA φ < 30° (*1*), FS φ < 35° N, L_s = 20°–90° and VIRA 75 (*2*) in comparison with averaged profiles obtained for the coldest regions of the cold collar (*3*) and the warmest regions at the latitude of the cold collar (*4*). (b) Temperature profiles VIRA 60 (*1*) and VIRA 75 (*2*) in comparison with averaged profiles obtained for the coldest regions of the cold collar (*3*) and the warmest regions at the latitude of the cold collar (*4*). (c) Correlation of temperature profiles for the North Pole region: (*1*) VIRA 85, (*2*) averaged profile IR V15, (*3*) the profiles of hot regions in 75–85° N and averaged profile according to IR V15, φ > 85° N (dashed line).

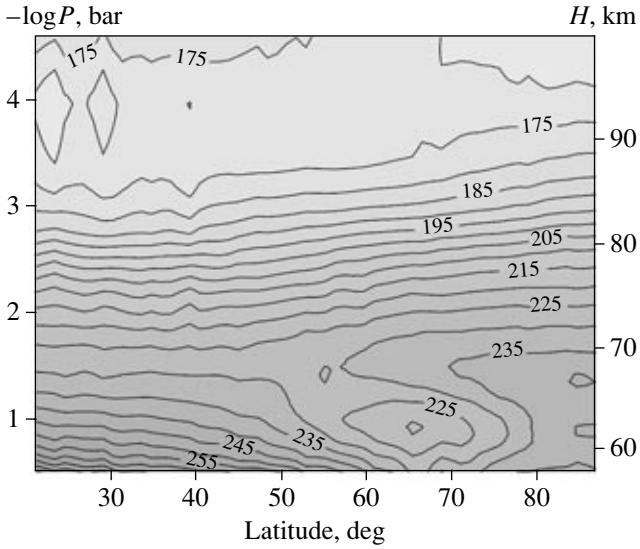

Fig. 12. Globally averaged temperature field derived from the data of IR spectrometry of *Venera-15*.

temperature profile for the hot dipole demonstrates higher temperature below 60 km in comparison with the surrounding near-polar region. However, near the level of 65 km the temperature in the hot dipole region is lower in the majority of cases. This difference depends on latitude and is a result of inversion existing in low latitudes at a height of 65 km.

Globally averaged temperature field is presented in Fig. 12a, and Figs. 13a–13d show the field averaged over quadrants of solar longitude. These data are averaged over 5° latitude intervals. In the globally averaged field (Fig. 12) one can clearly see an increase of temperature from low-latitude regions to the pole in the altitude range 65–90 km. At the level of about 95 km (in low latitudes) a temperature minimum is observed, which is related to temperature inversion. At high latitudes the temperature profiles are nearly isothermic. Below the level of 65 km temperature falls with latitude. This occurs up to latitude of 65°–70° where a temperature minimum associated with the cold collar is observed at altitudes of 64–65 km (the level of 100 mbar). In the polar region (φ > 80°) in the altitude interval 58–70 km temperature remains virtually constant (within 5 K).

The temperature fields averaged over measurements inside quadrants of solar longitude show that a strong latitude dependence of temperature is observed at isobaric levels in the morning time of the day (Fig. 13a) for L_s = 90°–20° (LT = 6:00–22:30). For example, at an altitude of about 80 km temperature varies from 180 K at low latitudes (20°–35°) up to 210 K at 87°. At higher altitudes, for these morning hours higher temperature values are typical. Near an altitude of 85 km (1 mbar level) a temperature minimum (175 K) is observed. At the level of 100 mbar one can well see the cold collar at latitude 65°. Low temperatures are observed in the near-polar region below 70 km.

In the afternoon time of the day (L_s = 310°–270°, LT = 13:30–18:00) an increase of temperature with latitude is observed, but only up to altitudes of 75–78 km.

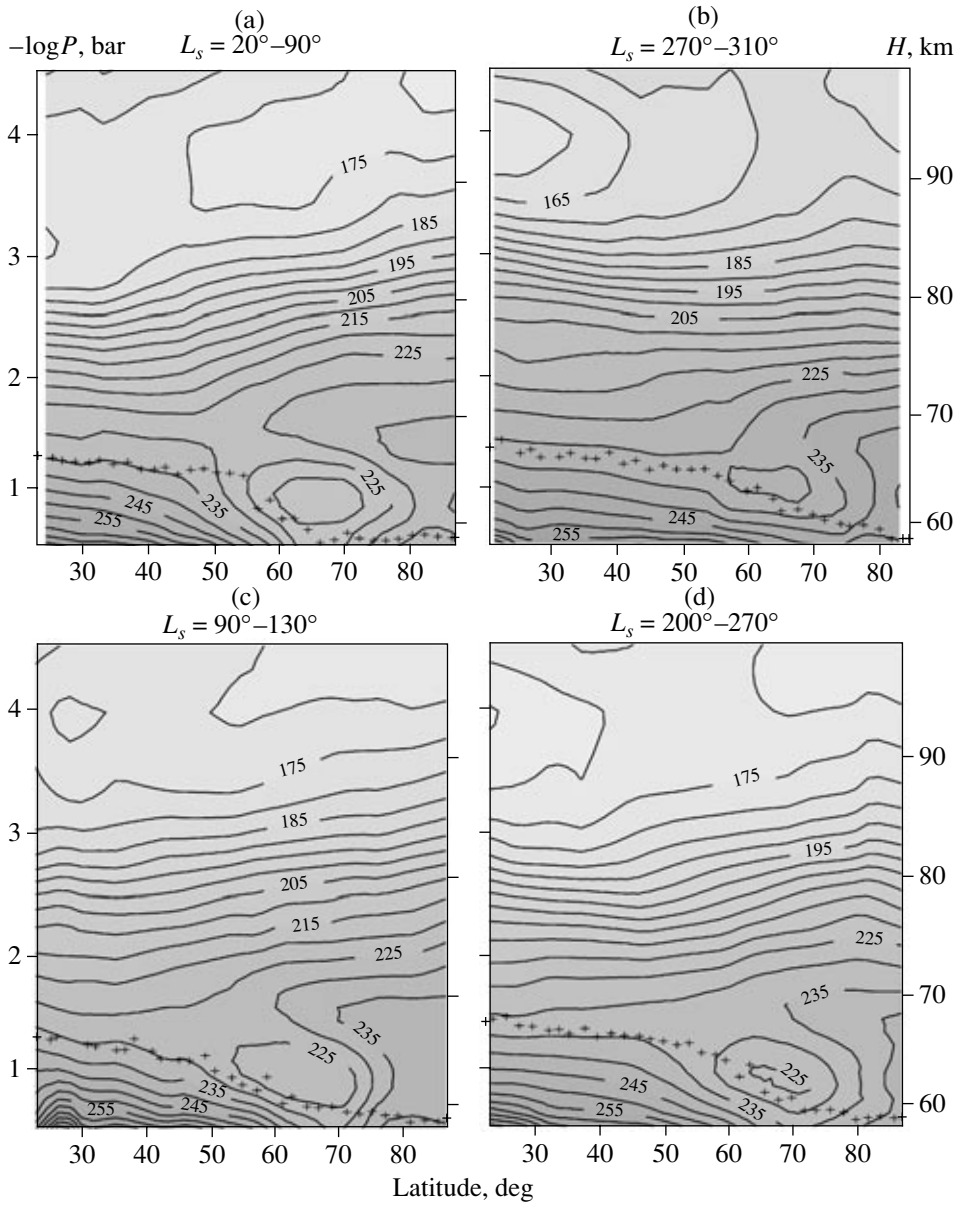

Fig. 13. The temperature field averaged over quadrants of solar longitude: (a) and (b) for the dayside, and (c) and (d) for the night side. Crosses mark the position of the upper boundary of clouds (ν = 1218 cm^{-1}).

The observed temperature at 80 km in the polar region is 200 K (for comparison, it is equal to 210 K on the morning side), while it is about 205 K at low latitudes (185 K in the morning). At low latitudes the atmosphere becomes warmer in comparison with morning hours. A temperature minimum (155 K) takes place at an altitude of 95 km in low latitudes. No cold collar can be isolated in this case. Above the pole the isothermic level corresponds to 245 K, which exceeds the morning temperature by 10 K.

During the day the atmosphere is heated at low latitudes in the altitude interval 75–85 km so that at the level of 80 km temperature increases from 175 K in the morning up to 200–205 K in the afternoon. At higher level the atmosphere is cooled so that at the altitude of 95 km temperature drops from 175–180 K in the morning down to 155–160 K in the afternoon. At altitudes of about 60 km the atmosphere in the morning is warmer than in the day (approximately, by 10 K). At high latitudes the largest variations of temperature are observed below 65 km. In the afternoon, temperature of the cold collar and polar regions is higher on the average by 10–15 K than in the morning.

At the segments adjacent to the evening terminator from the night side, in quadrants L_s = 270°–200°, LT = 18:00–22:30, and to the morning one, L_s = 130°–90°,

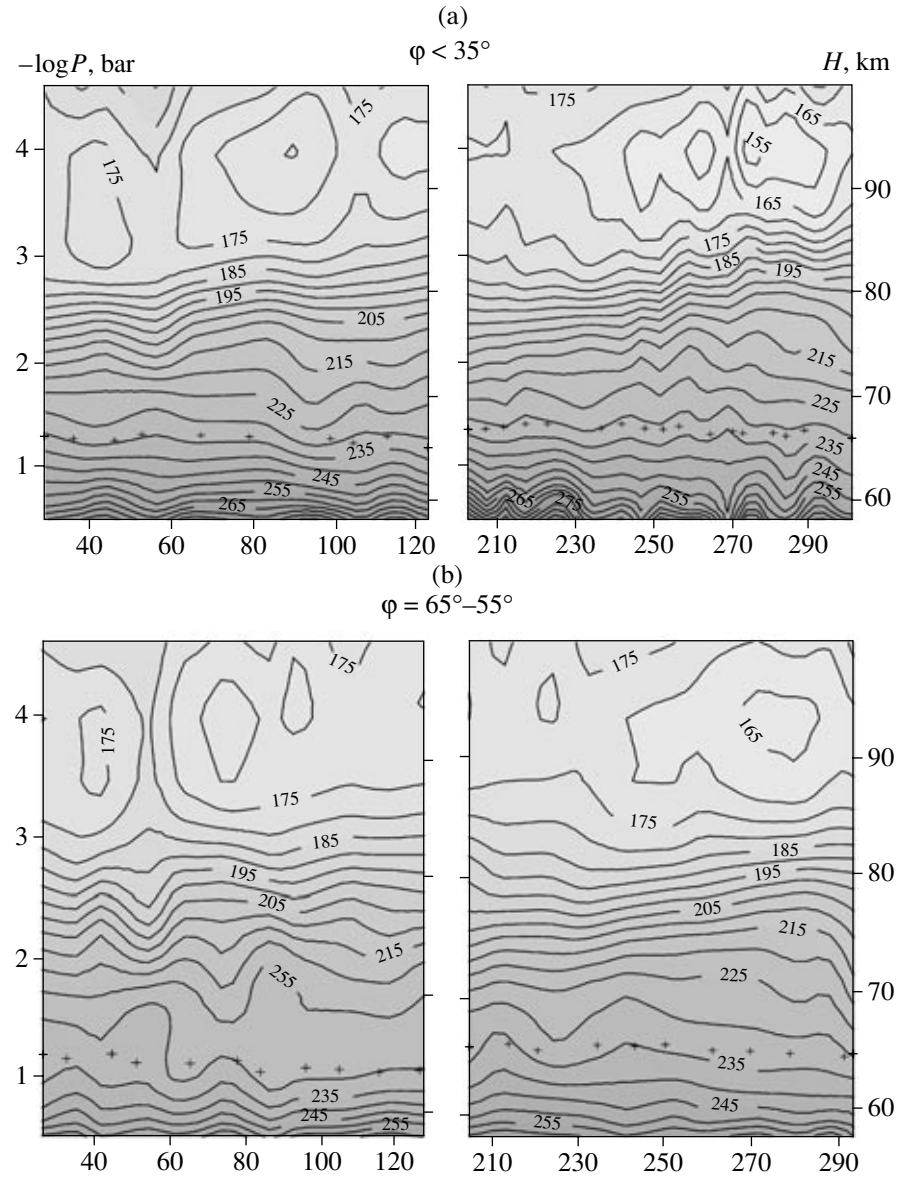

Fig. 14. The temperature field as a function of solar longitude and pressure averaged over intervals of 10° in L_s and in the latitude intervals accepted in VIRA 1; crosses mark location of the upper boundary of clouds.

LT = 3:30–6:00, the atmosphere is cooled at altitudes less than 70 km, and it is heated above 85 km.

The altitude of the upper boundary of clouds varies: it increases with decreasing temperature and is reduced at its growth.

The temperature fields as functions of solar longitude and pressure are presented in Fig. 14 for latitudes zones of the VIRA model. The thermal structure of the middle atmosphere of Venus in most intervals of altitude (see Figs. 13 and 14) strongly depends on latitude and local time. For a more detailed investigation we have selected 15 levels between 0.1 and 600 mbar (55–95 km) [33]. The altitude difference between the levels is chosen to be equal to 1–2 km in the cloud layer and 3–3.5 km above the level of clouds. The solar longitude (or local time) dependence of temperature on isobaric levels was represented in the form of Fourier series including five terms:

$$\begin{aligned} T(p, \phi, L_s) &= T_0(p, \phi) + T_1((p, \phi)\cos(L_s \\ &+ \varphi_1(p, \phi)) + T_2((p, \phi)\cos(2L_s + \varphi_2(p, \phi)) \\ &+ T_3((p, \phi)\cos(3L_s + \varphi_3(p, \phi)) \\ &+ T_4((p, \phi)\cos(4L_s + \varphi_4(p, \phi)), \end{aligned} \quad (1)$$

where p is pressure, ϕ is latitude, T_i and φ_i are the amplitude and phase of the ith harmonic, T_0 is the mean temperature, T_1 is the amplitude of the diurnal tidal

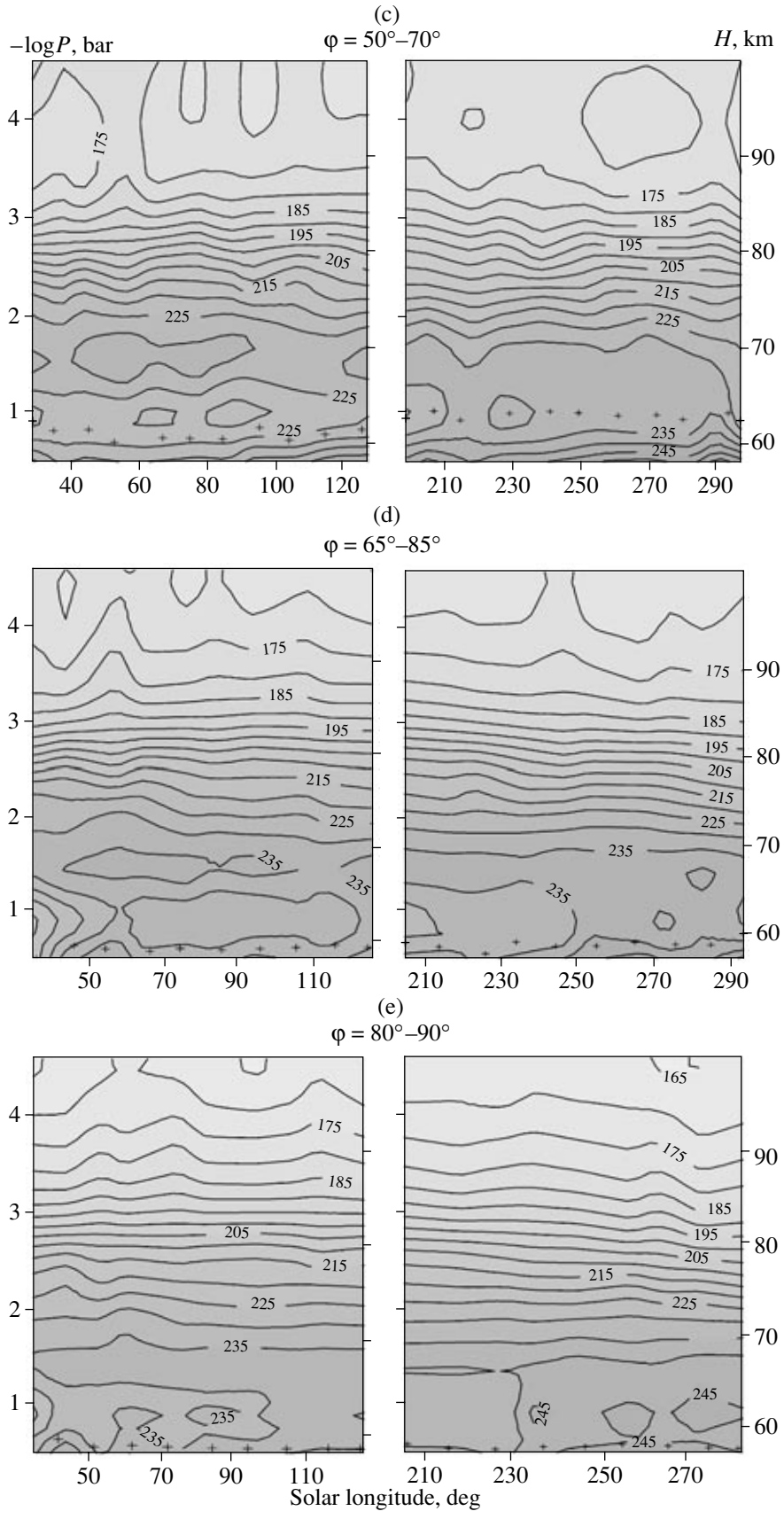

Fig. 14. (Contd.)

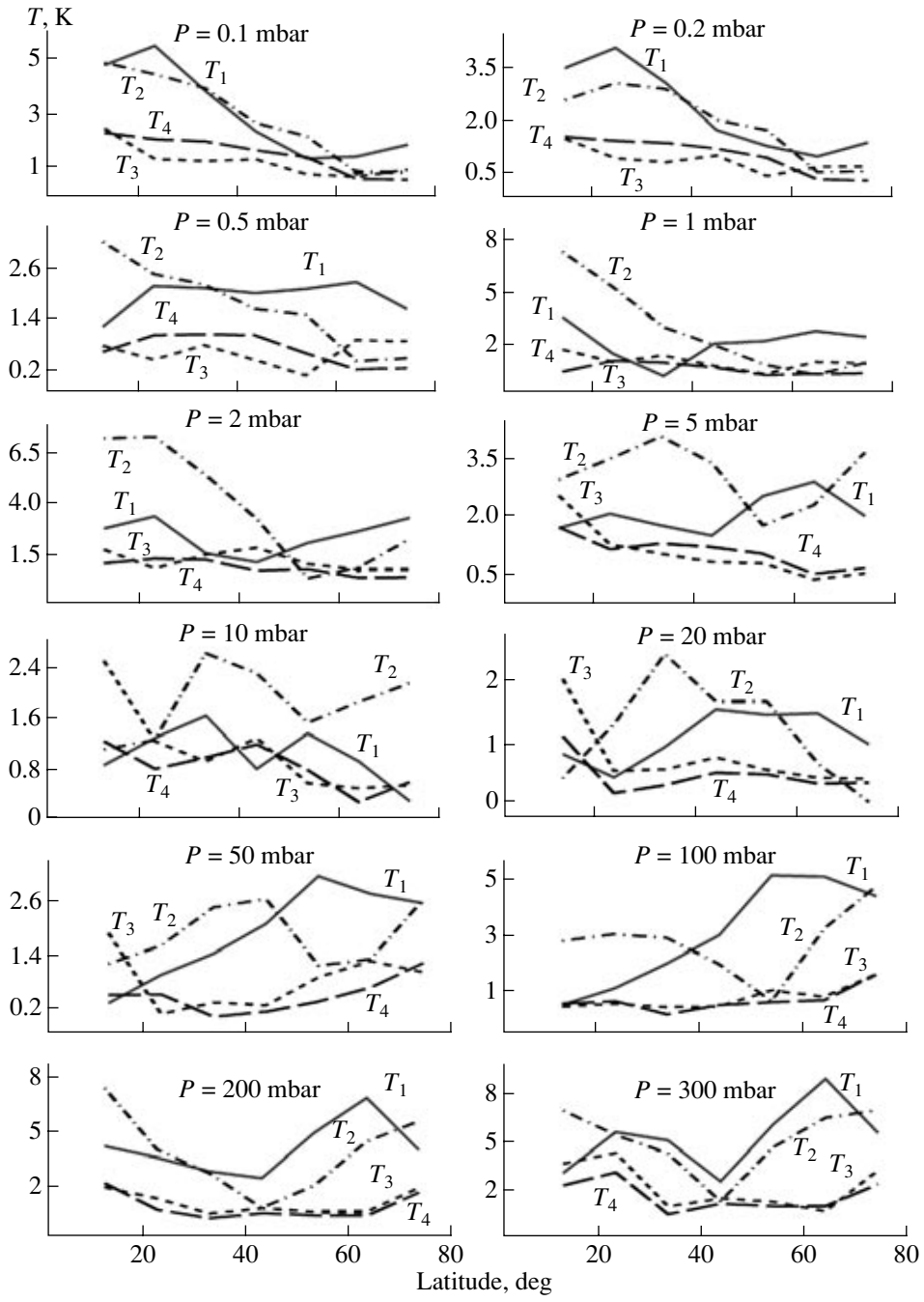

Fig. 15. The amplitudes of tidal components T_1–T_4 for several levels in the atmosphere.

wave, T_2 is the amplitude of semi-diurnal tidal wave, and so on. The amplitudes and phases depend on latitude and pressure (altitude).

Figure 15 demonstrates the variations of all four tidal components for isobaric levels in the range 0.1–300 mbar (95–58 km).

Taking all said above into account, we suggest a model of the middle atmosphere, depending on solar longitude (local time). Tables 2–6 present the vertical temperature profiles calculated by averaging the temperature profiles reconstructed according to spectra, solar longitude quadrants, and latitude intervals corresponding to the VIRA reference latitudes. The thermal structure of the Venusian atmosphere below 100 km, as it is described by the VIRA model, is generally confirmed by subsequent observations. The new data have made no radical changes; however, they include more information on temporal and spatial variations in the atmosphere. We have got a complicated pattern of lati-

Table 2

H, km	$\varphi < 35°$							
	$L_s = 20°–90°$		$L_s = 90°–130°$		$L_s = 200°–270°$		$L_s = 270°–310°$	
	P, bar	T, K	P, bar	T, K	P, bar	T, K	P, bar	T, K
100	$0.3069 \cdot 10^{-4}$	182.7	$0.2904 \cdot 10^{-4}$	173.8	$0.2861 \cdot 10^{-4}$	172.6	$0.2551 \cdot 10^{-4}$	167.8
99	$0.3929 \cdot 10^{-4}$	181.2	$0.3765 \cdot 10^{-4}$	172.5	$0.3717 \cdot 10^{-4}$	171.0	$0.3344 \cdot 10^{-4}$	164.7
98	$0.5041 \cdot 10^{-4}$	179.8	$0.4890 \cdot 10^{-4}$	171.5	$0.4840 \cdot 10^{-4}$	169.6	$0.4404 \cdot 10^{-4}$	162.2
97	$0.6480 \cdot 10^{-4}$	178.3	$0.6361 \cdot 10^{-4}$	170.6	$0.6317 \cdot 10^{-4}$	168.3	$0.5824 \cdot 10^{-4}$	159.9
96	$0.8351 \cdot 10^{-4}$	176.7	$0.8287 \cdot 10^{-4}$	169.7	$0.8261 \cdot 10^{-4}$	167.1	$0.7732 \cdot 10^{-4}$	157.9
95	$0.1079 \cdot 10^{-3}$	175.5	$0.1081 \cdot 10^{-3}$	169.4	$0.1082 \cdot 10^{-3}$	166.4	$0.1030 \cdot 10^{-3}$	156.6
94	$0.1394 \cdot 10^{-3}$	175.4	$0.1408 \cdot 10^{-3}$	170.4	$0.1417 \cdot 10^{-3}$	167.1	$0.1371 \cdot 10^{-3}$	158.2
93	$0.1802 \cdot 10^{-3}$	175.4	$0.1833 \cdot 10^{-3}$	171.3	$0.1854 \cdot 10^{-3}$	167.9	$0.1818 \cdot 10^{-3}$	160.1
92	$0.2329 \cdot 10^{-3}$	175.5	$0.2382 \cdot 10^{-3}$	172.2	$0.2423 \cdot 10^{-3}$	168.7	$0.2404 \cdot 10^{-3}$	162.1
91	$0.3011 \cdot 10^{-3}$	175.3	$0.3091 \cdot 10^{-3}$	173.2	$0.3162 \cdot 10^{-3}$	169.5	$0.3165 \cdot 10^{-3}$	164.8
90	$0.3894 \cdot 10^{-3}$	175.1	$0.4005 \cdot 10^{-3}$	174.3	$0.4121 \cdot 10^{-3}$	170.7	$0.4148 \cdot 10^{-3}$	168.3
89	$0.5038 \cdot 10^{-3}$	175.0	$0.5181 \cdot 10^{-3}$	175.8	$0.5360 \cdot 10^{-3}$	172.1	$0.5400 \cdot 10^{-3}$	172.7
88	$0.6521 \cdot 10^{-3}$	174.6	$0.6686 \cdot 10^{-3}$	177.5	$0.6955 \cdot 10^{-3}$	173.8	$0.6980 \cdot 10^{-3}$	177.9
87	$0.8439 \cdot 10^{-3}$	175.1	$0.8603 \cdot 10^{-3}$	180.0	$0.8997 \cdot 10^{-3}$	176.3	$0.8951 \cdot 10^{-3}$	183.8
86	$0.1091 \cdot 10^{-2}$	176.1	$0.1103 \cdot 10^{-2}$	182.8	$0.1159 \cdot 10^{-2}$	179.3	$0.1139 \cdot 10^{-2}$	189.4
85	$0.1408 \cdot 10^{-2}$	177.8	$0.1408 \cdot 10^{-2}$	186.1	$0.1487 \cdot 10^{-2}$	182.5	$0.1440 \cdot 10^{-2}$	194.6
84	$0.1811 \cdot 10^{-2}$	180.8	$0.1790 \cdot 10^{-2}$	189.9	$0.1898 \cdot 10^{-2}$	186.9	$0.1810 \cdot 10^{-2}$	199.2
83	$0.2316 \cdot 10^{-2}$	185.7	$0.2262 \cdot 10^{-2}$	194.7	$0.2408 \cdot 10^{-2}$	192.1	$0.2263 \cdot 10^{-2}$	203.8
82	$0.2942 \cdot 10^{-2}$	191.1	$0.2844 \cdot 10^{-2}$	199.0	$0.3035 \cdot 10^{-2}$	197.1	$0.2819 \cdot 10^{-2}$	206.9
81	$0.3712 \cdot 10^{-2}$	196.5	$0.3560 \cdot 10^{-2}$	203.0	$0.3805 \cdot 10^{-2}$	201.8	$0.3501 \cdot 10^{-2}$	209.4
80	$0.4655 \cdot 10^{-2}$	201.5	$0.4437 \cdot 10^{-2}$	206.4	$0.4746 \cdot 10^{-2}$	206.1	$0.4339 \cdot 10^{-2}$	211.4
79	$0.5809 \cdot 10^{-2}$	206.1	$0.5514 \cdot 10^{-2}$	209.1	$0.5895 \cdot 10^{-2}$	210.0	$0.5369 \cdot 10^{-2}$	212.9
78	$0.7214 \cdot 10^{-2}$	210.3	$0.6835 \cdot 10^{-2}$	211.5	$0.7297 \cdot 10^{-2}$	213.4	$0.6635 \cdot 10^{-2}$	214.3
77	$0.8927 \cdot 10^{-2}$	213.7	$0.8456 \cdot 10^{-2}$	213.3	$0.9005 \cdot 10^{-2}$	216.0	$0.8189 \cdot 10^{-2}$	215.5
76	$0.1101 \cdot 10^{-1}$	217.0	$0.1045 \cdot 10^{-1}$	215.0	$0.1109 \cdot 10^{-1}$	218.5	$0.1010 \cdot 10^{-1}$	216.8
75	$0.1354 \cdot 10^{-1}$	220.3	$0.1288 \cdot 10^{-1}$	217.1	$0.1362 \cdot 10^{-1}$	221.0	$0.1243 \cdot 10^{-1}$	218.7
74	$0.1660 \cdot 10^{-1}$	223.4	$0.1585 \cdot 10^{-1}$	219.3	$0.1670 \cdot 10^{-1}$	223.5	$0.1527 \cdot 10^{-1}$	221.1
73	$0.2031 \cdot 10^{-1}$	225.7	$0.1946 \cdot 10^{-1}$	221.2	$0.2043 \cdot 10^{-1}$	225.3	$0.1871 \cdot 10^{-1}$	223.2
72	$0.2480 \cdot 10^{-1}$	227.5	$0.2386 \cdot 10^{-1}$	222.9	$0.2496 \cdot 10^{-1}$	227.0	$0.2290 \cdot 10^{-1}$	225.1
71	$0.3024 \cdot 10^{-1}$	229.1	$0.2922 \cdot 10^{-1}$	224.5	$0.3045 \cdot 10^{-1}$	228.6	$0.2799 \cdot 10^{-1}$	226.9
70	$0.3683 \cdot 10^{-1}$	230.7	$0.3573 \cdot 10^{-1}$	226.2	$0.3709 \cdot 10^{-1}$	230.5	$0.3415 \cdot 10^{-1}$	228.6
69	$0.4479 \cdot 10^{-1}$	232.6	$0.4362 \cdot 10^{-1}$	228.1	$0.4511 \cdot 10^{-1}$	232.7	$0.4160 \cdot 10^{-1}$	230.5
68	$0.5438 \cdot 10^{-1}$	234.8	$0.5316 \cdot 10^{-1}$	230.2	$0.5475 \cdot 10^{-1}$	235.1	$0.5060 \cdot 10^{-1}$	232.5
67	$0.6590 \cdot 10^{-1}$	237.5	$0.6467 \cdot 10^{-1}$	232.8	$0.6632 \cdot 10^{-1}$	237.9	$0.6145 \cdot 10^{-1}$	234.5
66	$0.7967 \cdot 10^{-1}$	240.4	$0.7848 \cdot 10^{-1}$	235.6	$0.8016 \cdot 10^{-1}$	240.7	$0.7450 \cdot 10^{-1}$	236.8
65	$0.9609 \cdot 10^{-1}$	243.6	$0.9503 \cdot 10^{-1}$	238.8	$0.9668 \cdot 10^{-1}$	243.6	$0.9015 \cdot 10^{-1}$	239.1
64	0.1156	246.9	0.1148	242.3	0.1163	246.5	0.1089	241.5
63	0.1387	250.8	0.1382	246.4	0.1397	250.0	0.1313	244.2
62	0.1660	254.7	0.1658	250.8	0.1673	253.8	0.1579	247.2
61	0.1981	259.3	0.1983	256.2	0.1996	259.2	0.1895	250.9
60	0.2357	263.7	0.2363	262.0	0.2374	264.7	0.2268	254.6
59	0.2793	270.1	0.2803	269.5	0.2811	271.8	0.2706	260.0
58	0.3298	277.2	0.3308	278.0	0.3314	279.7	0.3215	267.0
57	0.3874	285.8	0.3883	287.3	0.3888	288.2	0.3800	275.7
56	0.4530	294.6	0.4537	295.9	0.4541	296.7	0.4466	285.6
55	0.5272	303.4	0.5277	304.5	0.5280	305.2	0.5221	295.6
54	0.6110	312.1	0.6113	313.0	0.6113	313.6	0.6071	305.6
53	0.7052	320.8	0.7054	321.5	0.7054	321.9	0.7026	315.6
52	0.8110	329.4	0.8110	329.9	0.8109	330.2	0.8095	325.6
51	0.9293	338.0	0.9292	338.2	0.9290	338.4	0.9286	335.7
50	1.061	347.4	1.060	347.4	1.060	347.4	1.060	346.8

Table 3

φ = 35°–55°								
H, km	L_s = 20°–90°		L_s = 90°–130°		L_s = 200°–270°		L_s = 270°–310°	
	P, bar	T, K	P, bar	T, K	P, bar	T, K	P, bar	T, K
100	$0.2653 \cdot 10^{-4}$	180.9	$0.2543 \cdot 10^{-4}$	173.0	$0.2638 \cdot 10^{-4}$	174.4	$0.2438 \cdot 10^{-4}$	172.3
99	$0.3405 \cdot 10^{-4}$	179.6	$0.3299 \cdot 10^{-4}$	172.3	$0.3415 \cdot 10^{-4}$	173.6	$0.3169 \cdot 10^{-4}$	170.7
98	$0.4378 \cdot 10^{-4}$	178.4	$0.4285 \cdot 10^{-4}$	171.7	$0.4427 \cdot 10^{-4}$	172.7	$0.4130 \cdot 10^{-4}$	169.0
97	$0.5637 \cdot 10^{-4}$	177.3	$0.5570 \cdot 10^{-4}$	171.2	$0.5748 \cdot 10^{-4}$	171.9	$0.5396 \cdot 10^{-4}$	167.6
96	$0.7273 \cdot 10^{-4}$	176.0	$0.7246 \cdot 10^{-4}$	170.7	$0.7472 \cdot 10^{-4}$	171.1	$0.7065 \cdot 10^{-4}$	166.2
95	$0.9401 \cdot 10^{-4}$	174.8	$0.9434 \cdot 10^{-4}$	170.3	$0.9725 \cdot 10^{-4}$	170.5	$0.9273 \cdot 10^{-4}$	165.0
94	$0.1216 \cdot 10^{-3}$	174.6	$0.1228 \cdot 10^{-3}$	170.8	$0.1266 \cdot 10^{-3}$	170.8	$0.1218 \cdot 10^{-3}$	165.1
93	$0.1574 \cdot 10^{-3}$	174.8	$0.1597 \cdot 10^{-3}$	171.6	$0.1647 \cdot 10^{-3}$	171.4	$0.1599 \cdot 10^{-3}$	165.7
92	$0.2036 \cdot 10^{-3}$	175.0	$0.2075 \cdot 10^{-3}$	172.3	$0.2141 \cdot 10^{-3}$	171.8	$0.2097 \cdot 10^{-3}$	166.3
91	$0.2633 \cdot 10^{-3}$	175.2	$0.2694 \cdot 10^{-3}$	173.0	$0.2781 \cdot 10^{-3}$	172.3	$0.2748 \cdot 10^{-3}$	166.9
90	$0.3405 \cdot 10^{-3}$	175.3	$0.3493 \cdot 10^{-3}$	173.8	$0.3611 \cdot 10^{-3}$	172.7	$0.3597 \cdot 10^{-3}$	167.7
89	$0.4401 \cdot 10^{-3}$	176.1	$0.4522 \cdot 10^{-3}$	175.4	$0.4683 \cdot 10^{-3}$	174.1	$0.4697 \cdot 10^{-3}$	169.8
88	$0.5678 \cdot 10^{-3}$	177.5	$0.5835 \cdot 10^{-3}$	177.7	$0.6059 \cdot 10^{-3}$	175.8	$0.6110 \cdot 10^{-3}$	172.7
87	$0.7311 \cdot 10^{-3}$	179.2	$0.7505 \cdot 10^{-3}$	180.3	$0.7817 \cdot 10^{-3}$	177.9	$0.7910 \cdot 10^{-3}$	176.3
86	$0.9387 \cdot 10^{-3}$	181.3	$0.9616 \cdot 10^{-3}$	183.3	$0.1006 \cdot 10^{-2}$	180.0	$0.1018 \cdot 10^{-2}$	180.4
85	$0.1202 \cdot 10^{-2}$	183.9	$0.1227 \cdot 10^{-2}$	186.7	$0.1289 \cdot 10^{-2}$	182.8	$0.1302 \cdot 10^{-2}$	185.3
84	$0.1532 \cdot 10^{-2}$	187.0	$0.1558 \cdot 10^{-2}$	190.4	$0.1646 \cdot 10^{-2}$	185.8	$0.1655 \cdot 10^{-2}$	190.5
83	$0.1946 \cdot 10^{-2}$	190.5	$0.1969 \cdot 10^{-2}$	194.3	$0.2094 \cdot 10^{-2}$	189.3	$0.2089 \cdot 10^{-2}$	196.0
82	$0.2460 \cdot 10^{-2}$	194.4	$0.2478 \cdot 10^{-2}$	198.1	$0.2651 \cdot 10^{-2}$	193.0	$0.2622 \cdot 10^{-2}$	200.9
81	$0.3095 \cdot 10^{-2}$	198.4	$0.3106 \cdot 10^{-2}$	201.5	$0.3341 \cdot 10^{-2}$	197.0	$0.3274 \cdot 10^{-2}$	205.0
80	$0.3876 \cdot 10^{-2}$	202.3	$0.3879 \cdot 10^{-2}$	204.7	$0.4190 \cdot 10^{-2}$	201.2	$0.4072 \cdot 10^{-2}$	208.5
79	$0.4835 \cdot 10^{-2}$	206.2	$0.4828 \cdot 10^{-2}$	207.8	$0.5230 \cdot 10^{-2}$	205.8	$0.5048 \cdot 10^{-2}$	211.7
78	$0.6006 \cdot 10^{-2}$	210.0	$0.5990 \cdot 10^{-2}$	211.0	$0.6497 \cdot 10^{-2}$	210.5	$0.6240 \cdot 10^{-2}$	214.5
77	$0.7435 \cdot 10^{-2}$	213.3	$0.7409 \cdot 10^{-2}$	213.9	$0.8035 \cdot 10^{-2}$	214.4	$0.7695 \cdot 10^{-2}$	216.7
76	$0.9178 \cdot 10^{-2}$	216.1	$0.9141 \cdot 10^{-2}$	216.4	$0.9903 \cdot 10^{-2}$	218.0	$0.9473 \cdot 10^{-2}$	218.4
75	$0.1130 \cdot 10^{-1}$	218.8	$0.1125 \cdot 10^{-1}$	218.8	$0.1217 \cdot 10^{-1}$	221.1	$0.1164 \cdot 10^{-1}$	220.1
74	$0.1388 \cdot 10^{-1}$	221.4	$0.1382 \cdot 10^{-1}$	220.9	$0.1491 \cdot 10^{-1}$	224.1	$0.1429 \cdot 10^{-1}$	221.7
73	$0.1700 \cdot 10^{-1}$	223.9	$0.1695 \cdot 10^{-1}$	222.6	$0.1822 \cdot 10^{-1}$	226.5	$0.1752 \cdot 10^{-1}$	223.0
72	$0.2079 \cdot 10^{-1}$	225.9	$0.2077 \cdot 10^{-1}$	223.8	$0.2224 \cdot 10^{-1}$	228.3	$0.2145 \cdot 10^{-1}$	224.3
71	$0.2539 \cdot 10^{-1}$	227.6	$0.2542 \cdot 10^{-1}$	224.8	$0.2710 \cdot 10^{-1}$	229.9	$0.2624 \cdot 10^{-1}$	225.7
70	$0.3097 \cdot 10^{-1}$	228.9	$0.3109 \cdot 10^{-1}$	225.5	$0.3298 \cdot 10^{-1}$	231.2	$0.3205 \cdot 10^{-1}$	227.1
69	$0.3774 \cdot 10^{-1}$	229.8	$0.3801 \cdot 10^{-1}$	226.0	$0.4011 \cdot 10^{-1}$	232.4	$0.3911 \cdot 10^{-1}$	228.5
68	$0.4596 \cdot 10^{-1}$	230.5	$0.4644 \cdot 10^{-1}$	226.6	$0.4874 \cdot 10^{-1}$	233.4	$0.4767 \cdot 10^{-1}$	230.0
67	$0.5595 \cdot 10^{-1}$	231.0	$0.5673 \cdot 10^{-1}$	227.3	$0.5916 \cdot 10^{-1}$	234.6	$0.5802 \cdot 10^{-1}$	231.5
66	$0.6809 \cdot 10^{-1}$	231.6	$0.6925 \cdot 10^{-1}$	228.0	$0.7175 \cdot 10^{-1}$	236.0	$0.7055 \cdot 10^{-1}$	232.9
65	$0.8281 \cdot 10^{-1}$	232.5	$0.8446 \cdot 10^{-1}$	229.2	$0.8691 \cdot 10^{-1}$	237.6	$0.8567 \cdot 10^{-1}$	234.6
64	0.1006	233.7	0.1029	231.1	0.1051	239.5	0.1039	236.5
63	0.1221	235.5	0.1251	233.7	0.1270	241.9	0.1257	238.8
62	0.1479	237.9	0.1517	237.2	0.1530	244.4	0.1519	241.4
61	0.1789	241.0	0.1833	241.9	0.1841	247.4	0.1831	244.7
60	0.2157	244.5	0.2207	247.1	0.2209	250.4	0.2202	248.3
59	0.2592	249.2	0.2646	254.1	0.2644	255.3	0.2639	253.8
58	0.3104	255.5	0.3154	261.9	0.3153	261.4	0.3148	260.5
57	0.3695	265.0	0.3739	271.6	0.3738	270.8	0.3735	270.1
56	0.4370	275.7	0.4405	281.6	0.4406	281.2	0.4404	280.5
55	0.5133	286.8	0.5159	291.9	0.5162	291.5	0.5161	291.0
54	0.5995	298.0	0.6010	302.2	0.6014	301.9	0.6015	301.5
53	0.6960	309.3	0.6966	312.6	0.6972	312.4	0.6974	312.0
52	0.8038	320.6	0.8035	323.0	0.8043	322.8	0.8046	322.6
51	0.9238	332.1	0.9227	333.5	0.9236	333.3	0.9241	333.2
50	1.056	344.7	1.054	344.9	1.055	344.8	1.056	344.9

Table 4

H, km	φ = 50°–70°							
	L_s = 20°–90°		L_s = 90°–130°		L_s = 200°–270°		L_s = 270°–310°	
	P, bar	T, K	P, bar	T, K	P, bar	T, K	P, bar	T, K
100	$0.2134 \cdot 10^{-4}$	177.8	$0.2185 \cdot 10^{-4}$	169.7	$0.2366 \cdot 10^{-4}$	171.6	$0.2335 \cdot 10^{-4}$	172.0
99	$0.2750 \cdot 10^{-4}$	176.7	$0.2848 \cdot 10^{-4}$	169.3	$0.3075 \cdot 10^{-4}$	171.1	$0.3035 \cdot 10^{-4}$	171.2
98	$0.3549 \cdot 10^{-4}$	175.9	$0.3714 \cdot 10^{-4}$	169.3	$0.3999 \cdot 10^{-4}$	170.9	$0.3948 \cdot 10^{-4}$	170.6
97	$0.4585 \cdot 10^{-4}$	175.3	$0.4843 \cdot 10^{-4}$	169.5	$0.5204 \cdot 10^{-4}$	170.7	$0.5141 \cdot 10^{-4}$	170.1
96	$0.5930 \cdot 10^{-4}$	174.6	$0.6314 \cdot 10^{-4}$	169.7	$0.6772 \cdot 10^{-4}$	170.6	$0.6700 \cdot 10^{-4}$	169.5
95	$0.7678 \cdot 10^{-4}$	173.8	$0.8228 \cdot 10^{-4}$	170.0	$0.8816 \cdot 10^{-4}$	170.6	$0.8740 \cdot 10^{-4}$	169.0
94	$0.9951 \cdot 10^{-4}$	173.3	$0.1072 \cdot 10^{-3}$	170.6	$0.1147 \cdot 10^{-3}$	171.0	$0.1141 \cdot 10^{-3}$	169.1
93	$0.1290 \cdot 10^{-3}$	173.5	$0.1394 \cdot 10^{-3}$	171.5	$0.1492 \cdot 10^{-3}$	171.8	$0.1488 \cdot 10^{-3}$	169.6
92	$0.1672 \cdot 10^{-3}$	173.8	$0.1811 \cdot 10^{-3}$	172.5	$0.1937 \cdot 10^{-3}$	172.7	$0.1940 \cdot 10^{-3}$	170.1
91	$0.2166 \cdot 10^{-3}$	174.3	$0.2349 \cdot 10^{-3}$	173.5	$0.2513 \cdot 10^{-3}$	173.5	$0.2526 \cdot 10^{-3}$	170.7
90	$0.2804 \cdot 10^{-3}$	174.7	$0.3043 \cdot 10^{-3}$	174.6	$0.3256 \cdot 10^{-3}$	174.2	$0.3287 \cdot 10^{-3}$	171.4
89	$0.3628 \cdot 10^{-3}$	175.1	$0.3934 \cdot 10^{-3}$	176.2	$0.4213 \cdot 10^{-3}$	175.6	$0.4272 \cdot 10^{-3}$	172.8
88	$0.4687 \cdot 10^{-3}$	176.9	$0.5072 \cdot 10^{-3}$	178.5	$0.5436 \cdot 10^{-3}$	177.9	$0.5535 \cdot 10^{-3}$	175.0
87	$0.6037 \cdot 10^{-3}$	179.1	$0.6515 \cdot 10^{-3}$	181.3	$0.6990 \cdot 10^{-3}$	180.4	$0.7145 \cdot 10^{-3}$	177.7
86	$0.7750 \cdot 10^{-3}$	181.9	$0.8336 \cdot 10^{-3}$	184.4	$0.8956 \cdot 10^{-3}$	183.2	$0.9186 \cdot 10^{-3}$	180.9
85	$0.9908 \cdot 10^{-3}$	184.9	$0.1062 \cdot 10^{-2}$	188.0	$0.1143 \cdot 10^{-2}$	186.5	$0.1175 \cdot 10^{-2}$	184.7
84	$0.1261 \cdot 10^{-2}$	189.1	$0.1346 \cdot 10^{-2}$	192.1	$0.1452 \cdot 10^{-2}$	190.5	$0.1496 \cdot 10^{-2}$	189.0
83	$0.1596 \cdot 10^{-2}$	193.6	$0.1697 \cdot 10^{-2}$	196.4	$0.1835 \cdot 10^{-2}$	194.4	$0.1893 \cdot 10^{-2}$	193.7
82	$0.2008 \cdot 10^{-2}$	198.4	$0.2130 \cdot 10^{-2}$	200.5	$0.2309 \cdot 10^{-2}$	198.2	$0.2383 \cdot 10^{-2}$	198.2
81	$0.2514 \cdot 10^{-2}$	203.1	$0.2662 \cdot 10^{-2}$	203.9	$0.2893 \cdot 10^{-2}$	201.7	$0.2984 \cdot 10^{-2}$	202.5
80	$0.3131 \cdot 10^{-2}$	207.6	$0.3316 \cdot 10^{-2}$	207.0	$0.3611 \cdot 10^{-2}$	205.2	$0.3721 \cdot 10^{-2}$	206.4
79	$0.3882 \cdot 10^{-2}$	211.7	$0.4118 \cdot 10^{-2}$	210.0	$0.4492 \cdot 10^{-2}$	208.6	$0.4621 \cdot 10^{-2}$	210.0
78	$0.4797 \cdot 10^{-2}$	215.3	$0.5100 \cdot 10^{-2}$	212.6	$0.5567 \cdot 10^{-2}$	212.2	$0.5720 \cdot 10^{-2}$	213.4
77	$0.5907 \cdot 10^{-2}$	218.7	$0.6299 \cdot 10^{-2}$	215.3	$0.6875 \cdot 10^{-2}$	215.8	$0.7057 \cdot 10^{-2}$	216.6
76	$0.7253 \cdot 10^{-2}$	221.4	$0.7760 \cdot 10^{-2}$	218.2	$0.8463 \cdot 10^{-2}$	219.3	$0.8683 \cdot 10^{-2}$	219.4
75	$0.8887 \cdot 10^{-2}$	223.8	$0.9535 \cdot 10^{-2}$	221.0	$0.1038 \cdot 10^{-2}$	222.6	$0.1066 \cdot 10^{-2}$	222.0
74	$0.1087 \cdot 10^{-2}$	225.9	$0.1169 \cdot 10^{-1}$	223.6	$0.1271 \cdot 10^{-1}$	225.4	$0.1305 \cdot 10^{-1}$	224.3
73	$0.1327 \cdot 10^{-1}$	227.8	$0.1429 \cdot 10^{-1}$	226.0	$0.1551 \cdot 10^{-1}$	228.0	$0.1595 \cdot 10^{-1}$	226.4
72	$0.1617 \cdot 10^{-1}$	229.3	$0.1744 \cdot 10^{-1}$	228.0	$0.1890 \cdot 10^{-1}$	230.1	$0.1947 \cdot 10^{-1}$	228.1
71	$0.1970 \cdot 10^{-1}$	230.5	$0.2127 \cdot 10^{-1}$	229.4	$0.2300 \cdot 10^{-1}$	231.6	$0.2373 \cdot 10^{-1}$	229.5
70	$0.2397 \cdot 10^{-1}$	231.1	$0.2590 \cdot 10^{-1}$	230.2	$0.2796 \cdot 10^{-1}$	232.6	$0.2890 \cdot 10^{-1}$	230.6
69	$0.2917 \cdot 10^{-1}$	231.2	$0.3154 \cdot 10^{-1}$	230.3	$0.3397 \cdot 10^{-1}$	232.9	$0.3517 \cdot 10^{-1}$	231.2
68	$0.3551 \cdot 10^{-1}$	230.4	$0.3842 \cdot 10^{-1}$	229.5	$0.4129 \cdot 10^{-1}$	232.6	$0.4280 \cdot 10^{-1}$	231.4
67	$0.4327 \cdot 10^{-1}$	228.8	$0.4686 \cdot 10^{-1}$	228.0	$0.5021 \cdot 10^{-1}$	231.7	$0.5207 \cdot 10^{-1}$	231.2
66	$0.5283 \cdot 10^{-1}$	226.5	$0.5725 \cdot 10^{-1}$	226.1	$0.6112 \cdot 10^{-1}$	230.5	$0.6339 \cdot 10^{-1}$	230.8
65	$0.6465 \cdot 10^{-1}$	224.1	$0.7006 \cdot 10^{-1}$	224.2	$0.7447 \cdot 10^{-1}$	229.4	$0.7720 \cdot 10^{-1}$	230.3
64	$0.7929 \cdot 10^{-1}$	221.8	$0.8588 \cdot 10^{-1}$	222.8	$0.9083 \cdot 10^{-1}$	228.6	$0.9404 \cdot 10^{-1}$	230.5
63	$0.9742 \cdot 10^{-1}$	220.1	0.1053	222.5	0.1108	228.7	0.1145	231.4
62	0.1198	220.2	0.1291	223.8	0.1351	230.1	0.1392	233.6
61	0.1472	221.1	0.1580	226.6	0.1644	232.8	0.1689	236.8
60	0.1806	224.0	0.1927	230.8	0.1996	236.4	0.2042	241.0
59	0.2209	226.6	0.2342	235.4	0.2415	240.0	0.2461	245.8
58	0.2696	229.7	0.2835	240.0	0.2914	244.1	0.2955	251.1
57	0.3283	232.7	0.3419	245.3	0.3500	251.6	0.3532	257.5
56	0.3983	238.1	0.4103	253.3	0.4177	261.7	0.4202	265.4
55	0.4793	252.1	0.4886	266.0	0.4947	274.0	0.4968	276.7
54	0.5703	268.3	0.5768	279.9	0.5815	286.6	0.5831	289.0
53	0.6716	285.0	0.6753	294.1	0.6787	299.5	0.6799	301.4
52	0.7835	302.2	0.7848	308.7	0.7871	312.6	0.7879	313.9
51	0.9062	319.9	0.9058	323.6	0.9072	325.8	0.9077	326.7
50	1.039	338.5	1.038	339.2	1.039	339.9	1.039	340.1

Table 5

φ = 70°–80°								
H, km	L_s = 20°–90°		L_s = 90°–130°		L_s = 200°–270°		L_s = 270°–310°	
	P, bar	T, K	P, bar	T, K	P, bar	T, K	P, bar	T, K
100	$0.2504 \cdot 10^{-4}$	171.9	$0.2480 \cdot 10^{-4}$	166.8	$0.2554 \cdot 10^{-4}$	168.0	$0.2557 \cdot 10^{-4}$	168.9
99	$0.3253 \cdot 10^{-4}$	171.4	$0.3246 \cdot 10^{-4}$	167.0	$0.3338 \cdot 10^{-4}$	167.8	$0.3336 \cdot 10^{-4}$	168.8
98	$0.4227 \cdot 10^{-4}$	171.7	$0.4246 \cdot 10^{-4}$	167.7	$0.4360 \cdot 10^{-4}$	168.4	$0.4353 \cdot 10^{-4}$	169.1
97	$0.5490 \cdot 10^{-4}$	172.2	$0.5547 \cdot 10^{-4}$	168.7	$0.5691 \cdot 10^{-4}$	169.1	$0.5676 \cdot 10^{-4}$	169.6
96	$0.7126 \cdot 10^{-4}$	172.6	$0.7234 \cdot 10^{-4}$	169.8	$0.7419 \cdot 10^{-4}$	169.9	$0.7396 \cdot 10^{-4}$	170.0
95	$0.9243 \cdot 10^{-4}$	173.2	$0.9419 \cdot 10^{-4}$	170.9	$0.9661 \cdot 10^{-4}$	170.7	$0.9632 \cdot 10^{-4}$	170.5
94	$0.1198 \cdot 10^{-3}$	174.1	$0.1224 \cdot 10^{-3}$	172.3	$0.1256 \cdot 10^{-3}$	171.9	$0.1253 \cdot 10^{-3}$	171.3
93	$0.1549 \cdot 10^{-3}$	175.3	$0.1588 \cdot 10^{-3}$	173.8	$0.1630 \cdot 10^{-3}$	173.4	$0.1628 \cdot 10^{-3}$	172.4
92	$0.2001 \cdot 10^{-3}$	176.6	$0.2054 \cdot 10^{-3}$	175.4	$0.2110 \cdot 10^{-3}$	174.9	$0.2112 \cdot 10^{-3}$	173.6
91	$0.2580 \cdot 10^{-3}$	177.9	$0.2652 \cdot 10^{-3}$	177.0	$0.2727 \cdot 10^{-3}$	176.5	$0.2735 \cdot 10^{-3}$	174.8
90	$0.3320 \cdot 10^{-3}$	179.1	$0.3416 \cdot 10^{-3}$	178.7	$0.3515 \cdot 10^{-3}$	178.0	$0.3535 \cdot 10^{-3}$	176.2
89	$0.4265 \cdot 10^{-3}$	180.7	$0.4389 \cdot 10^{-3}$	180.7	$0.4521 \cdot 10^{-3}$	180.0	$0.4559 \cdot 10^{-3}$	177.9
88	$0.5463 \cdot 10^{-3}$	183.1	$0.5621 \cdot 10^{-3}$	183.2	$0.5795 \cdot 10^{-3}$	182.7	$0.5864 \cdot 10^{-3}$	180.0
87	$0.6974 \cdot 10^{-3}$	185.8	$0.7174 \cdot 10^{-3}$	186.1	$0.7401 \cdot 10^{-3}$	185.6	$0.7519 \cdot 10^{-3}$	182.5
86	$0.8869 \cdot 10^{-3}$	189.0	$0.9120 \cdot 10^{-3}$	189.4	$0.9413 \cdot 10^{-3}$	189.0	$0.9606 \cdot 10^{-3}$	185.4
85	$0.1123 \cdot 10^{-2}$	192.5	$0.1154 \cdot 10^{-2}$	193.0	$0.1192 \cdot 10^{-2}$	192.8	$0.1222 \cdot 10^{-2}$	188.8
84	$0.1416 \cdot 10^{-2}$	197.0	$0.1454 \cdot 10^{-2}$	197.2	$0.1501 \cdot 10^{-2}$	197.4	$0.1548 \cdot 10^{-2}$	192.7
83	$0.1775 \cdot 10^{-2}$	201.7	$0.1823 \cdot 10^{-2}$	201.5	$0.1882 \cdot 10^{-2}$	202.0	$0.1951 \cdot 10^{-2}$	196.9
82	$0.2213 \cdot 10^{-2}$	206.5	$0.2275 \cdot 10^{-2}$	205.4	$0.2346 \cdot 10^{-2}$	206.5	$0.2447 \cdot 10^{-2}$	200.9
81	$0.2747 \cdot 10^{-2}$	211.0	$0.2828 \cdot 10^{-2}$	208.7	$0.2913 \cdot 10^{-2}$	210.3	$0.3057 \cdot 10^{-2}$	204.8
80	$0.3394 \cdot 10^{-2}$	215.0	$0.3506 \cdot 10^{-2}$	211.6	$0.3604 \cdot 10^{-2}$	213.6	$0.3803 \cdot 10^{-2}$	208.5
79	$0.4180 \cdot 10^{-2}$	218.5	$0.4335 \cdot 10^{-2}$	214.2	$0.4446 \cdot 10^{-2}$	216.4	$0.4713 \cdot 10^{-2}$	211.9
78	$0.5133 \cdot 10^{-2}$	221.4	$0.5347 \cdot 10^{-2}$	216.4	$0.5471 \cdot 10^{-2}$	219.0	$0.5824 \cdot 10^{-2}$	215.2
77	$0.6289 \cdot 10^{-2}$	223.7	$0.6582 \cdot 10^{-2}$	218.8	$0.6717 \cdot 10^{-2}$	221.5	$0.7171 \cdot 10^{-2}$	218.7
76	$0.7691 \cdot 10^{-2}$	225.9	$0.8082 \cdot 10^{-2}$	221.5	$0.8226 \cdot 10^{-2}$	224.5	$0.8803 \cdot 10^{-2}$	222.2
75	$0.9386 \cdot 10^{-2}$	228.1	$0.9900 \cdot 10^{-2}$	224.2	$0.1005 \cdot 10^{-1}$	227.3	$0.1077 \cdot 10^{-1}$	225.4
74	$0.1144 \cdot 10^{-1}$	229.5	$0.1210 \cdot 10^{-1}$	226.8	$0.1225 \cdot 10^{-1}$	229.4	$0.1315 \cdot 10^{-1}$	228.3
73	$0.1393 \cdot 10^{-1}$	230.9	$0.1476 \cdot 10^{-1}$	229.1	$0.1491 \cdot 10^{-1}$	231.3	$0.1601 \cdot 10^{-1}$	230.9
72	$0.1694 \cdot 10^{-1}$	232.0	$0.1796 \cdot 10^{-1}$	231.4	$0.1812 \cdot 10^{-1}$	233.1	$0.1946 \cdot 10^{-1}$	233.3
71	$0.2058 \cdot 10^{-1}$	233.4	$0.2182 \cdot 10^{-1}$	233.6	$0.2199 \cdot 10^{-1}$	234.9	$0.2361 \cdot 10^{-1}$	235.3
70	$0.2498 \cdot 10^{-1}$	234.4	$0.2647 \cdot 10^{-1}$	235.4	$0.2666 \cdot 10^{-1}$	236.3	$0.2861 \cdot 10^{-1}$	237.0
69	$0.3030 \cdot 10^{-1}$	235.3	$0.3207 \cdot 10^{-1}$	237.0	$0.3228 \cdot 10^{-1}$	237.5	$0.3462 \cdot 10^{-1}$	238.4
68	$0.3674 \cdot 10^{-1}$	235.2	$0.3883 \cdot 10^{-1}$	237.5	$0.3907 \cdot 10^{-1}$	237.7	$0.4186 \cdot 10^{-1}$	238.9
67	$0.4459 \cdot 10^{-1}$	234.1	$0.4703 \cdot 10^{-1}$	236.5	$0.4731 \cdot 10^{-1}$	236.8	$0.5063 \cdot 10^{-1}$	238.4
66	$0.5420 \cdot 10^{-1}$	231.7	$0.5703 \cdot 10^{-1}$	234.8	$0.5736 \cdot 10^{-1}$	235.1	$0.6128 \cdot 10^{-1}$	237.5
65	$0.6602 \cdot 10^{-1}$	229.2	$0.6927 \cdot 10^{-1}$	233.0	$0.6964 \cdot 10^{-1}$	233.6	$0.7423 \cdot 10^{-1}$	236.6
64	$0.8060 \cdot 10^{-1}$	226.8	$0.8425 \cdot 10^{-1}$	231.6	$0.8464 \cdot 10^{-1}$	232.5	$0.8998 \cdot 10^{-1}$	236.1
63	$0.9859 \cdot 10^{-1}$	225.1	0.1026	230.9	0.1030	231.8	0.1091	235.9
62	0.1207	224.6	0.1249	230.9	0.1253	231.5	0.1323	236.2
61	0.1478	224.6	0.1521	231.2	0.1525	231.4	0.1603	237.1
60	0.1808	226.5	0.1850	232.4	0.1856	232.4	0.1941	238.8
59	0.2208	229.0	0.2248	234.4	0.2255	234.4	0.2345	241.4
58	0.2690	231.2	0.2727	236.6	0.2735	236.6	0.2827	244.8
57	0.3273	233.2	0.3303	238.8	0.3311	240.3	0.3399	249.8
56	0.3952	248.1	0.3972	253.1	0.3976	254.4	0.4055	263.2
55	0.4715	264.0	0.4725	267.9	0.4727	268.9	0.4797	276.3
54	0.5570	279.1	0.5571	281.9	0.5570	282.7	0.5631	288.8
53	0.6525	293.4	0.6517	295.3	0.6514	295.8	0.6567	300.7
52	0.7588	307.0	0.7574	308.1	0.7570	308.4	0.7615	312.3
51	0.8768	320.1	0.8750	320.4	0.8744	320.4	0.8783	323.4
50	1.007	332.6	1.006	332.2	1.005	332.1	1.008	334.2

Table 6

φ = 85°								
H, km	L_s = 20°–90°		L_s = 90°–130°		L_s = 200°–270°		L_s = 270°–310°	
	P, bar	T, K	P, bar	T, K	P, bar	T, K	P, bar	T, K
100	$0.2682 \cdot 10^{-4}$	168.3	$0.2654 \cdot 10^{-4}$	166.2	$0.2699 \cdot 10^{-4}$	167.1	$0.2523 \cdot 10^{-4}$	165.5
99	$0.3503 \cdot 10^{-4}$	168.3	$0.3477 \cdot 10^{-4}$	166.4	$0.3531 \cdot 10^{-4}$	167.3	$0.3310 \cdot 10^{-4}$	165.5
98	$0.4572 \cdot 10^{-4}$	169.2	$0.4551 \cdot 10^{-4}$	167.4	$0.4615 \cdot 10^{-4}$	168.2	$0.4340 \cdot 10^{-4}$	166.1
97	$0.5958 \cdot 10^{-4}$	170.2	$0.5946 \cdot 10^{-4}$	168.7	$0.6023 \cdot 10^{-4}$	169.3	$0.5685 \cdot 10^{-4}$	166.9
96	$0.7753 \cdot 10^{-4}$	171.2	$0.7754 \cdot 10^{-4}$	170.0	$0.7847 \cdot 10^{-4}$	170.4	$0.7438 \cdot 10^{-4}$	167.7
95	$0.1007 \cdot 10^{-3}$	172.5	$0.1009 \cdot 10^{-3}$	171.5	$0.1021 \cdot 10^{-3}$	171.7	$0.9719 \cdot 10^{-4}$	168.6
94	$0.1305 \cdot 10^{-3}$	174.2	$0.1309 \cdot 10^{-3}$	173.4	$0.1325 \cdot 10^{-3}$	173.3	$0.1268 \cdot 10^{-3}$	169.7
93	$0.1688 \cdot 10^{-3}$	176.1	$0.1695 \cdot 10^{-3}$	175.3	$0.1715 \cdot 10^{-3}$	175.0	$0.1651 \cdot 10^{-3}$	171.1
92	$0.2176 \cdot 10^{-3}$	177.9	$0.2188 \cdot 10^{-3}$	177.2	$0.2215 \cdot 10^{-3}$	176.7	$0.2145 \cdot 10^{-3}$	172.7
91	$0.2798 \cdot 10^{-3}$	179.8	$0.2816 \cdot 10^{-3}$	179.2	$0.2854 \cdot 10^{-3}$	178.5	$0.2780 \cdot 10^{-3}$	174.3
90	$0.3589 \cdot 10^{-3}$	181.9	$0.3615 \cdot 10^{-3}$	181.2	$0.3667 \cdot 10^{-3}$	180.3	$0.3595 \cdot 10^{-3}$	176.0
89	$0.4590 \cdot 10^{-3}$	184.2	$0.4628 \cdot 10^{-3}$	183.6	$0.4700 \cdot 10^{-3}$	182.6	$0.4636 \cdot 10^{-3}$	178.1
88	$0.5849 \cdot 10^{-3}$	187.3	$0.5902 \cdot 10^{-3}$	186.6	$0.6003 \cdot 10^{-3}$	185.4	$0.5960 \cdot 10^{-3}$	180.5
87	$0.7424 \cdot 10^{-3}$	190.6	$0.7498 \cdot 10^{-3}$	189.7	$0.7639 \cdot 10^{-3}$	188.5	$0.7636 \cdot 10^{-3}$	183.1
86	$0.9383 \cdot 10^{-3}$	194.0	$0.9487 \cdot 10^{-3}$	193.1	$0.9681 \cdot 10^{-3}$	191.7	$0.9748 \cdot 10^{-3}$	185.9
85	$0.1181 \cdot 10^{-2}$	197.9	$0.1195 \cdot 10^{-2}$	196.8	$0.1222 \cdot 10^{-2}$	195.5	$0.1240 \cdot 10^{-2}$	189.1
84	$0.1479 \cdot 10^{-2}$	202.5	$0.1499 \cdot 10^{-2}$	201.1	$0.1535 \cdot 10^{-2}$	199.7	$0.1570 \cdot 10^{-2}$	192.8
83	$0.1843 \cdot 10^{-2}$	206.9	$0.1871 \cdot 10^{-2}$	205.3	$0.1919 \cdot 10^{-2}$	204.0	$0.1978 \cdot 10^{-2}$	196.8
82	$0.2287 \cdot 10^{-2}$	211.1	$0.2326 \cdot 10^{-2}$	209.1	$0.2388 \cdot 10^{-2}$	207.9	$0.2482 \cdot 10^{-2}$	200.7
81	$0.2826 \cdot 10^{-2}$	214.4	$0.2882 \cdot 10^{-2}$	212.2	$0.2962 \cdot 10^{-2}$	211.3	$0.3101 \cdot 10^{-2}$	204.3
80	$0.3484 \cdot 10^{-2}$	217.0	$0.3560 \cdot 10^{-2}$	214.6	$0.3662 \cdot 10^{-2}$	214.1	$0.3860 \cdot 10^{-2}$	208.1
79	$0.4286 \cdot 10^{-2}$	219.2	$0.4389 \cdot 10^{-2}$	216.9	$0.4515 \cdot 10^{-2}$	216.9	$0.4785 \cdot 10^{-2}$	211.9
78	$0.5262 \cdot 10^{-2}$	221.3	$0.5400 \cdot 10^{-2}$	219.3	$0.5554 \cdot 10^{-2}$	219.6	$0.5910 \cdot 10^{-2}$	215.9
77	$0.6449 \cdot 10^{-2}$	223.3	$0.6628 \cdot 10^{-2}$	221.6	$0.6814 \cdot 10^{-2}$	222.3	$0.7270 \cdot 10^{-2}$	220.1
76	$0.7887 \cdot 10^{-2}$	225.7	$0.8119 \cdot 10^{-2}$	224.2	$0.8341 \cdot 10^{-2}$	225.0	$0.8911 \cdot 10^{-2}$	223.9
75	$0.9626 \cdot 10^{-2}$	228.3	$0.9922 \cdot 10^{-2}$	226.7	$0.1019 \cdot 10^{-1}$	227.5	$0.1089 \cdot 10^{-1}$	227.3
74	$0.1173 \cdot 10^{-1}$	230.0	$0.1210 \cdot 10^{-1}$	228.7	$0.1241 \cdot 10^{-1}$	229.6	$0.1327 \cdot 10^{-1}$	230.0
73	$0.1427 \cdot 10^{-1}$	231.6	$0.1474 \cdot 10^{-1}$	230.6	$0.1511 \cdot 10^{-1}$	231.4	$0.1614 \cdot 10^{-1}$	232.4
72	$0.1734 \cdot 10^{-1}$	232.7	$0.1793 \cdot 10^{-1}$	232.2	$0.1836 \cdot 10^{-1}$	233.2	$0.1959 \cdot 10^{-1}$	234.9
71	$0.2106 \cdot 10^{-1}$	234.1	$0.2177 \cdot 10^{-1}$	234.2	$0.2228 \cdot 10^{-1}$	235.2	$0.2373 \cdot 10^{-1}$	237.1
70	$0.2554 \cdot 10^{-1}$	235.6	$0.2639 \cdot 10^{-1}$	236.3	$0.2699 \cdot 10^{-1}$	237.2	$0.2870 \cdot 10^{-1}$	239.5
69	$0.3094 \cdot 10^{-1}$	237.1	$0.3194 \cdot 10^{-1}$	238.4	$0.3264 \cdot 10^{-1}$	239.3	$0.3464 \cdot 10^{-1}$	241.8
68	$0.3745 \cdot 10^{-1}$	237.9	$0.3861 \cdot 10^{-1}$	239.7	$0.3943 \cdot 10^{-1}$	240.5	$0.4177 \cdot 10^{-1}$	243.1
67	$0.4533 \cdot 10^{-1}$	237.5	$0.4666 \cdot 10^{-1}$	239.5	$0.4762 \cdot 10^{-1}$	240.4	$0.5033 \cdot 10^{-1}$	243.4
66	$0.5493 \cdot 10^{-1}$	235.5	$0.5643 \cdot 10^{-1}$	238.2	$0.5755 \cdot 10^{-1}$	239.3	$0.6066 \cdot 10^{-1}$	243.4
65	$0.6668 \cdot 10^{-1}$	234.0	$0.6832 \cdot 10^{-1}$	237.6	$0.6960 \cdot 10^{-1}$	239.0	$0.7309 \cdot 10^{-1}$	243.8
64	$0.8099 \cdot 10^{-1}$	233.4	$0.8271 \cdot 10^{-1}$	237.8	$0.8417 \cdot 10^{-1}$	239.3	$0.8803 \cdot 10^{-1}$	244.8
63	$0.9841 \cdot 10^{-1}$	233.5	0.1001	238.5	0.1017	240.2	0.1059	245.8
62	0.1195	234.5	0.1211	239.7	0.1229	241.0	0.1275	245.7
61	0.1451	233.9	0.1464	238.7	0.1485	239.9	0.1534	244.8
60	0.1763	233.4	0.1773	237.5	0.1796	238.8	0.1849	243.4
59	0.2141	235.1	0.2147	238.2	0.2173	239.3	0.2230	243.0
58	0.2597	236.5	0.2597	239.5	0.2626	240.6	0.2688	244.6
57	0.3145	238.6	0.3138	241.5	0.3170	242.7	0.3236	245.7
56	0.3806	240.7	0.3791	242.3	0.3824	244.8	0.3890	250.9
55	0.4565	256.8	0.4543	257.6	0.4575	259.9	0.4635	265.3
54	0.5416	272.0	0.5390	272.1	0.5420	274.2	0.5474	278.9
53	0.6370	286.4	0.6340	285.8	0.6368	287.9	0.6416	291.9
52	0.7434	300.1	0.7402	299.0	0.7427	300.8	0.7469	304.4
51	0.8619	313.2	0.8588	311.6	0.8610	313.3	0.8645	316.4
50	0.9934	325.7	0.9906	323.8	0.9924	325.3	0.9953	327.9

tude and temporal variations. We present a family of model vertical profiles of the middle atmosphere that take into account local time dependence. There are no analogs of such a dependence in the original Vira model.

ACKNOWLEDGMENTS

We thank the Russian Foundation for Basic Research for financial support (project no. 01-02-17481).

REFERENCES

1. Moroz, V.I., Huntress, W.H., and Shevalev, I.L., Planetary Missions in the 20th Century, *Kosm. Issled.*, 2002, vol. 40, no. 5, pp. 451–481.
2. Huntress, W.H., Moroz, V.I., and Shevalev, I.L., Lunar and Planetary Robotic and Exploration Missions in the 20th Century, *Space Sci. Rev.*, 2002, vol. 107, no. 3, pp. 541–649.
3. Kliore, A., Moroz, V.I., and Keating, G., The Venus International Reference Atmosphere, *Adv. Space Res.*, 1985, no. 11.
4. Seiff, A., Schofield, J.T., Kliore, A.J., et al., Models of the Structure of the Atmosphere of Venus from the Surface to 100 km Altitude, *Adv. Space Res.*, 1985, vol. 5, no. 11, pp. 3–58.
5. Oertel, D., Moroz, V.I., Linkin, V.M., et al., Infrared Experiment on *Venera-15* and *Venera-16* Orbital Stations: 1. Methods and First Results, *Kosm. Issled.*, 1985, vol. 23, pp. 191–205.
6. Oertel, D., Moroz, V.I., Spankuch, D., et al., Infrared Spectrometry from Venera-15 and Venera-16, *Adv. Space Res.*, 1987, vol. 5, p. 25.
7. Moroz, V.I., Oertel, D., Linkin, V.M., et al., Venus Spacecraft's Infrared Radiance Spectra and Some Aspects of Their Interpretation, *Appl. Opt.*, 1986, vol. 25, pp. 1710–1719.
8. Yakovlev, O.I., Gubenko, V.N., Matygov, S.S., et al., Venusian Atmosphere in the Southern Near-Polar Region, *Kosm. Issled.*, 1987, vol. 25, pp. 258–266.
9. Yakovlev, O.I., Matygov, S.S., Efimov, A.I., et al., Venusian Atmosphere in the Northern Polar Region, *Kosm. Issled.*, 1987, vol. 25, pp. 267–274.
10. Yakovlev, O.I., Matygov, S.S., and Gubenko, V.N., Venera-15 and 16 Middle Atmosphere Profiles from Radar Occultations: Polar and Near-Polar Atmosphere of Venus, *Icarus,* 1991, vol. 94, pp. 493–510.
11. Linkin, V.M., Kerzhanovich, V.V., Lipatov, A.N., et al., Thermal Structure of the Venus Atmosphere in the Middle Cloud Layer, *Science*, 1986, vol. 231, pp. 1420–1422.
12. Linkin, V.M., Blamon, J., Devyatkin, S.I., et al., Thermal Structure of the Atmosphere of Venus according to the Data of Measurements by Landing Vehicle *Vega-2*, *Kosm. Issled.*, 1987, vol. 25, no. 5, pp. 659–672.
13. Crisp, D., Ingersoll, A.P., Hildebrand, C.E., and Prenston, R.A., VEGA Balloon Meteorological Measurements, *Adv. Space Res.*, 1990, vol. 10, pp. 109–124.
14. Belton, J.S., Gierasch, P.J., Smith, M.D., et al., Images from Galileo of the Venus Cloud Deck, *Science*, 1991, vol. 253, pp. 1531–1536.
15. Carlson, R.W., Baines, K.H., Encrenaz, Th., et al., Galileo Infrared Imaging Spectroscopy Measurements at Venus, *Science*, 1991, vol. 253, pp. 1541–1548.
16. Drossart, P.B., Bézard, B.Th., Encrenaz, Th., et al.,Search for Spatial Variations of the H_2O Abundance in the Lower Atmosphere of Venus from NIMS-Galileo, *Planet. Space Sci.,* 1993, vol. 41, pp. 495–504.
17. Grinspoon, D.H., Pollack, J.B., Sitton, B.R., et al., Probing Venus' Cloud Structure with Galileo-NIMS, *Planet. Space Sci.*, 1993, vol. 41, pp. 515–542.
18. Roos-Serote, M., Drossart, P., Encrenaz, Th., et al., The Thermal Structure and Dynamics of the Atmosphere of Venus between 70–90 km from the Galileo-NIMS Spectra, *Icarus*, 1995, vol. 114, pp. 300–309.
19. Bezard, B., de Bergh, C., Crisp, D., and Maillard, J.-P., The Deep Atmosphere of Venus Revealed by High-Resolution Nightside Spectra, *Nature*, 1990, vol. 345, pp. 508–511.
20. Pollack, J.B., Dalton, J., Grinspoon, D., et al., Near-Infrared Light from Venus' Nightside—A Spectroscopic Analysis, *Icarus,* 1993, vol. 103, pp. 1–42.
21. Taylor, F.W., Crisp, D., and Bezard, B., Near Infrared Sounding of the Lower Atmosphere of Venus, in *Venus II*, Tucson, Arizona: Univ. of Arizona Press, 1997, pp. 325–352.
22. Hinson, D. and Jenkins, V., Magellan Radio Occultation Measurements of Atmospheric Waves on Venus, *Icarus,* 1995, vol. 114, p. 310.
23. Baines, K.H., Bellucci, G., Bibring, J.-P., et al., Detection of Sub-Micron Radiation from the Surface of Venus by Cassini/VIMS, *Icarus*, 2000, vol. 148, pp. 307–311.
24. Kliore, A. and Patel, V., Thermal Structure of the Atmosphere of Venus from Pioneer Venus Radio Occultations, *Icarus*, 1982, vol. 52, pp. 320–334.
25. Kliore, A.J., Recent Results on Venus Atmosphere from Pioneer Venus Radio Occultations, *Adv. Space Res.*, 1985, vol. 5, no. 9, pp. 41–49.
26. Moroz, V.I. and Zasova, L.V., VIRA-2: A Review of Inputs for Updating the Venus International Reference Atmosphere, *Adv. Space Res.*, 1997, vol. 19, no. 8, pp. 1191–1201.
27. Schafer, K., Zasova, L.V., Spankuch, D., et al., Structure of the Middle Atmosphere of Venus from Analyses of Fourier-Spectrometer Measurements aboard Venera-15, *Adv. Space Res.*, 1987, vol. 7, no. 12, pp. 17–24.
28. Schafer, K., Dubois, R., Haus, R., et al., Infrared Fourier Spectrometer Experiment from Venera-15, *Adv. Space Res.*, 1990, vol. 10, no. 5, pp. 57–66.
29. Schafer, K., Linkin, V.M., Dethloff, K., et al., Temperature and Thermal Wind Field of the Middle Atmosphere of Venus from Venera-15 Data, in *Veroffenlichungen des Forschungsbereichs Geo- und Kosmoswissenschaften*, Berlin: Academie-Verlag, 1990.
30. Zasova, L.V., The Structure of the Venusian Atmosphere at High Latitudes, *Adv. Space Res.,* 1995, vol. 16, pp. 89–98.
31. Zasova, L.V., Moroz, V.I., and Linkin, V.M., Venera-15, 16 and VEGA Missions as Sources for Improvements of

the Venus Reference Atmosphere, *Adv. Space Res.*, 1996, vol. 17, no. 11, pp. 171–180.

32. Zasova, L.V., Khatountsev, I.A., Moroz, V.I., and Ignatiev, N.I., Structure of the Venus Middle Atmosphere: Venera 15 Fourier Spectrometry Data Revisited, *Adv. Space Res.*, 1999, vol. 23, no. 9, pp. 1559–1568.
33. Zasova, L.V., Khatuntsev, I.V., Ignatiev, N.I., and Moroz, V.I., Local Time Variations of the Middle Atmosphere of Venus: Solar-Related Structures, *Adv. Space Res.*, 2002, vol. 299, no. 2, pp. 243–248.
34. Zasova, L.V., Moroz, V.I., Formisano, V., et al., Infrared Spectrometry of Venus: IR Fourier Spectrometer on Venera 15 as a Precursor of PFS for Venus Express, *Adv. Space Res.*, 2004, vol. 34, pp. 1655–1667.
35. Zasova, L.V., Ignatiev, N.I., Khatuntsev, I.V., and Linkin, V.M., Structure of the Venus Atmosphere, *Planet. Space Sci.*, 2006, in press.
36. Seiff, A., Kirk, D., Young, R., et al., Measurements of Thermal Structure and Thermal Contrasts in the Atmosphere of Venus and Related Dynamic Observations: Results from the Four Pioneer Venus Probes, *J. Geophys. Res.*, 1980, vol. 85 A, pp. 7903–7933.